Optimization and Characterization of a Laser Engraving System for Carbon-Based Electronic Devices

A thesis presented to

the faculty of

the Russ College of Engineering and Technology of Ohio University

In partial fulfillment

of the requirements for the degree

Master of Science

Tianyi Cai

May 2019

© 2019 Tianyi Cai. All Rights Reserved.

This thesis titled

Optimization and Characterization of a Laser Engraving System for Carbon-Based Electronic Devices

by

TIANYI CAI

has been approved for

the School of Electrical Engineering and Computer Science

and the Russ College of Engineering and Technology by

Savas Kaya

Professor of Electrical Engineering and Computer Science

Dennis Irwin

Dean, Russ College of Engineering and Technology

ABSTRACT

CAI TIANYI, M.S., May 2019, Electrical Engineering

Optimization and Characterization of a Laser Engraving System for Carbon-Based Electronic Devices

Director of Thesis: Savas Kaya

Flexible electronics has become a burgeoning research field, and it has shown high potential in the industrial field due to its material and functional flexibility, as well as its low cost and environmentally-friendly features. Predominantly additive printing-based technologies have been utilized to fabricate flexible electronics on various substrates. Direct laser-writing is an alternative approach that can selectively modify the surface of a layer to form lasting chemical or physical changes that can further lower cost and expand fabrication toolsets for high-resolution flexible devices. The first part of this thesis methodically explores a low-cost compact laser scribing or engraving tool that carbonizes the surface of polyimide polymer (Kapton®), paper, and wood layers that turned into conductive upon irradiation. The optimal drive parameters for the blue-violet laser (λ=445nm) scriber with ~0.5mm beam size are shown to have a linear speed of 1200mm/min, laser power of 60 unit (~0.75W) and line spacing of 16line/mm. In addition, the carbon allotropic composition and lifetime of produced conductive layers were investigated. The second part of this thesis focuses on applications of the laser scribed conductive layers for electrical components. Passive resistors and capacitors, possessing different designing parameters, were fabricated and tested. Moreover, working examples of resistive strain sensors and a three-electrode electrochemical cells are

fabricated using the laser engraver, which demonstrate the industrial relevance and extremely attractive features of this method.

DEDICATION

I would first like to dedicate this thesis to my parents, Cai Bo and Sun Guimei. Without their love and support, I would never have had opportunities to achieve my dreams. I would also like to dedicate this work to my wife, Lulu. She has provided me encouragement and support to become a better person.

ACKNOWLEDGMENTS

I first want to sincerely thank my advisor, Dr. Savas Kaya, since without his support and help, this work would not have been finished. He has helped and motivated me through the entire process of the project. Beyond the technical aspects, he has also taught me to become a responsible person. I also would like to thank the rest of my committee members: Dr. Wojciech Jadwisienczak, Dr. Avinash Karanth, and Dr. David Tees. They provided valuable help and accelerated the accomplishing of this work.

I also want to give credit to my colleagues, Jason Wright, Parthiban Rajan, and Akanksha Rohit. They have shared their valuable academic and practical experience with me.

Finally, I would like to thank a special person, my uncle Sun Hongfa. He is not only an outstanding scientist, but also a person who inspired my interest in natural science.

TABLE OF CONTENTS

Page

LIST OF TABLES

LIST OF FIGURES

CHAPTER 1: INTRODUCTION

1.1 Motivation

Printed electronics on flexible substrates represents one of the most promising and innovative technologies today; it offers a flexible, light-weight, and low-cost integration platform suitable for multiple applications and disciplines. The fundamental elements of flexible electronics include a flexible substrate on which conductive and insulating materials can be attached or deposited selectively. To create conductive patterns or electrodes on a substrate, a high-resolution printer or solution dispensing system is typically used. Many such systems have been developed in past decades. Although printing is a relatively simpler and highly-capable approach to fabricate electronics, as compared to conventional silicon chip technologies, the method has some inherent limitations. First, the resolution is limited to ~20 microns by the nature of solution delivery to the surface. Secondly, the quality, purity, and particle size of nano-particle based ink and flatness of the substrate significantly affects the product quality. However, utilization of high-quality ink and ultra-flat pure substrates increases the cost. Thirdly, curing of ink varies from material to material and requires extra time and effort.

Recently, researchers have used a direct laser beam to partially carbonize polymer substrates and form a conductive layer composed by carbon allotropes, without using any conductive ink [1] [2]. Such use of laser-scribing to form conductive lines avoids any of the above complications and further simplifies an already low-cost technology in principle. Accordingly, I explore this new approach in this thesis, investigating its potential and limits by use of a low-cost table-top laser engraving system on a number of substrates.

This thesis explores the optimization of a one-step laser-writing process to directly fabricate conductive carbon layers and electrodes on polyimide (Kapton®) and paper by a solid-state blue-violet laser (445nm). We examine how the writing parameters impact the electrical properties of the conductive carbon allotrope layer and the performance of electrodes in passive electronic components such as resistors and capacitors. Subsequently, the more complex and functional devices, an electrochemical sensor and strain sensor, are also fabricated, tested, and compared with conventional sensors.

1.2 Flexible Electronics

Flexible electronics has been rapidly developing in the past two decades; it has become a promising technology which is capable of being applied to multiple fields because of its tolerance to deformation, small size, ultra-light weight, and low cost. The first generation of flexible electronics was typically passive and single functional; a typical example is printed radio-frequency identification (RFID) devices with printed antennas. Those devices usually exclude power or data storage modules; and they must be made extremely low-cost. With the evolution of technology, new generation of flexible electronics have become more complicated and more functional; furthermore, besides passive (*R, L, C*) circuit elements, contemporary flexible electronics is capable of forming and integrating a wide range of electronic system components, such as printed transistors as well as flexible displays, solar cells, and batteries [8]. As a result, modern flexible electronics has become a complete integration platform, and such integrated devices are capable of accomplishing many complex tasks independently. Although in most cases, the resulting flexible electronic systems cannot compete with conventional

semiconductor chips in performance, they maintain a distinct advantage in terms of cost, large-area capability, and ability to conform to complex shapes and curved surfaces, which enables unique solutions and products.

Figure 1. Selected typical flexible electronics fabricating by different methods [3] [4] [5]

As a very promising form of technology, flexible electronics can be applied in many fields of practical interest. Utilization of flexible electronics in healthcare and medical research, often integrated to wearable products or harnesses, is considered especially revolutionary. Wearable devices that collect physical or medical data as people go about their daily life are expected to significantly increase the efficiency of and reduce the cost of healthcare. Based on a flexible (polymer, textile, or even skin) substrate and low-cost circuitry, wearable devices can include conventional surface-mount components as well as fully flexible electronics. Figure 1(a) shows a sweat sensor that can be used to diagnose cystic fibrosis [3]. The printed circuits board (PCB) was eliminated to tolerate moderate bending deformation, and the whole device was capsuled in flexible elastomer (PDMS) in order to wrap around the wrist. Nevertheless, the device cannot bear too much shear stress, and flexible PCB also has a limited ability to rebound when continuous force is applied. Figure 1(b) shows a LED circuitry directly printed on the back-hand skin [4]. Because all components are attached to skin, the whole circuitry can survive rapid

deformation. Directly printing on skin is typically intended for time-limited applications and can be affected by numerous factors. More complicated circuitry requires longer printing times and a more stable working surface, but user hold less stable with time cumulating. Figure 1(c) demonstrates another type of flexible electronics; by combining PCB-free electronics and flexible electronics, a flexible substrate encapsulates the circuits made by liquid or solid metal [5]. A gallium alloy appears in a liquid phase at room temperature, and Galinstan (liquid Ga product), is injected into the microchannels in the substrate as liquid wire to operate as conductive pathways with higher capacity for deformation.

Flexible PCB, 3-D printed flexible electronics, and encapsulated flexible electronics function very well, but the cost of those types of devices is still high, so mass production and marketing will be restricted. Furthermore, the design and manufacture of such types of electronics contain numerous technical difficulties because of the knowledge gap about new conductive materials. Depositing or printing nanoinks on a flexible substrate is still more practical, and today it has been largely adapted in industrial fields. However, as indicated earlier, printing itself can have resolution and ink-dependent limitations. For instance, the pressure and motion sensor in Figure 2 (a) illustrates a printed electronic sensing device with wires and electrodes that are directly deployed on a flexible substrate instead of modified PCB [6]. Compared to devices in Figure 1, this type of flexible electronics offers both an excellent contact surface and large area applications with more complex shapes. In this case, a network of strain sensors is created on the finger surface so as to quantify the location and amount of

pressure. However, the design of circuitry can be more complicated in order to accomplish such complex tasks.

Aside from the elimination of PCB and formation of complex shapes, flexible electronics also offers a number of new devices such as broadband and highly-tuned antennas, displays, solar cells, LEDs, and batteries that can also be formed using printing technologies on polymer substrates. As shown in Figure 2b, a fully flexible OLED screen developed by LG, there are many published works [8] that utilize these capabilities and expand the applications for flexible electronics. Although still lacking in performance and capacity, these novel elements allow flexible electronics to be proposed for many novel wearable and low-cost solutions. In this thesis, the proposed laser-mediated carbonization process is another tool that can further expand the capabilities of the flexible electronics, simplify the fabrication process, and lower costs even further.

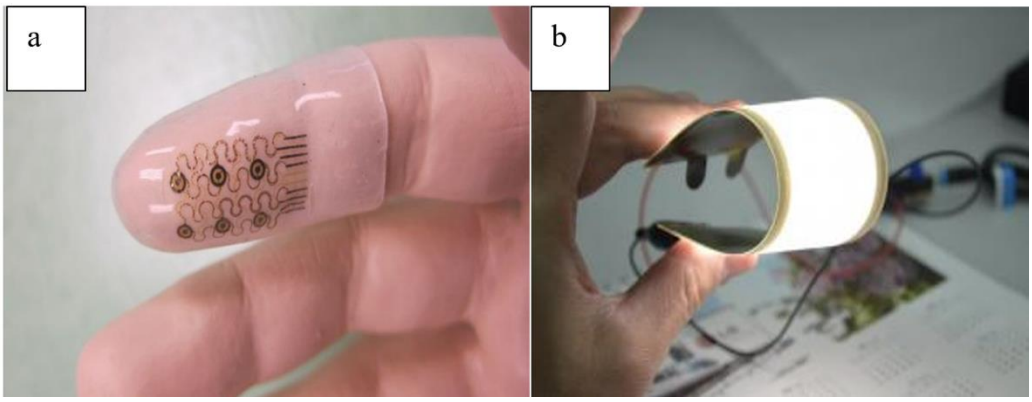

Figure 2. Prototype of printed flexible electronics (a) pressure sensor (b) OLED display [6] [7]

1.3 Market Analysis of Flexible Electronics

Although flexible electronics is an emerging technology, the market for flexible electronic has grown steadily in the last decade, as shown in Figure 3 (a). Moreover, it is predicted that market revenue of flexible electronics will retain this rate of growth and reach $16.50 billion in 2021. Figure 3(b) shows the percentages of various types of flexible electronics; personal care devices include wearable devices and medical devices, which will contribute more than 75% of the total flexible electronics revenue by 2021 [8] [9]. Therefore, wearable/flexible devices have the potential to become a critical part of everyday consumer products and ongoing expansion of personalized medicine as the population increases. In addition to this, other important developments such as smart systems that utilize sensor readings to become aware of their surrounding and adapt to new situations can also bring considerable expansion for flexible electronics [8].

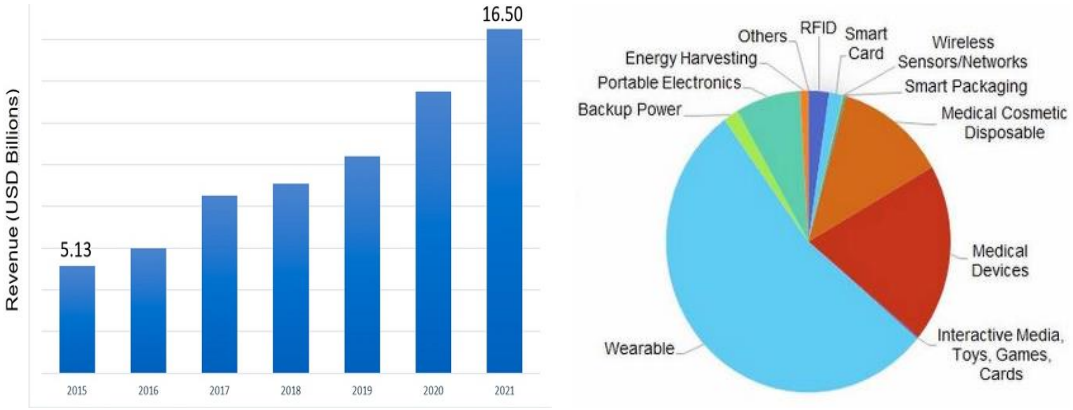

Figure 3. Prediction of global flexible electronics market revenue [9]

Researchers predict the actual marketing revenue will grow beyond expectation because other research areas are also rapidly developing. For example, biomedical sensors have been used to perform only a single monitoring function. However, since more biomarkers have been discovered and characterized as medical knowledge expands,

the newest generation of biomedical sensors can perform more complicated multi-modal diagnostic functions. Researchers have started to develop flexible electronic devices which are capable of executing drug delivery and other therapeutic functions. [10]

Market growth in flexible electronics directly stimulates the industries involved in the fabrication of flexible devices. Such industries rely on low-cost and high-efficiency facilities and processes to achieve mass production which can satisfy market demand. Hence, the development of new processes is critical to the growth of flexible electronics.

1.4 Thesis Goals

Existing studies have presented the possibility of producing a conductive layer on the surface of Kapton film using a laser engraving system or laser cutter [1]. Carbon allotropes contain carbon black, graphite, graphite oxide, graphene oxide, graphene and other possible allotropes which constitute the conductive layer on Kapton surfaces after laser burning [1]. Those studies also showed that when the Kapton surface burned in a specific pattern, the conductive layer acted as wires to compose functional electronics. However, those studies have not provided a detailed process description that can lead to fabrication of optimal resistance layers. Moreover, previous works only experimented with polyimide, and no other materials were used to check the implications of the laser scribe process. This thesis addresses these gaps in the process optimization and material studies. Subsequently, it illustrates the practical value of the developed process on several practical devices. Therefore, the three specific goals of the thesis are:

- Goal 1: Development and optimization of the laser carbonization process on flexible media.

- Goal 2: Exploration of different media that can take advantage of the laser carbonization process
- Goal 3: Illustration of the potential of the developed process on practical devices.

1.5 Thesis Organization and Achievements

In line with the above objectives, after introducing the relevant background and tools used in the study, the thesis examines in Chapter 3 the laser process parameters and the resulting carbonized layer structures in order to identify the optimal burning conditions. It also explores the aging of the resulting devices in air. Chapter 4 uses these process conditions to build capacitive devices, an electrochemical sensor, and a bending sensor to illustrate the examples of devices that can be built with the process developed.

Besides developing a well-described and optimized process via a low-cost laser engraver, the thesis also examines the possibility of forming a carbon layer on other organic substrates, paper and cardboard, as the use of paper/carboard as a substrate for laser carbonization is a very novel feature of this work and has not been explored earlier. Similarly, the previously published research works do not examine the lifetime of laser engraved devices, which is another unique aspect of this work

CHAPTER 2: BACKGROUND

2.1 History

Lasers were initially used to reduce graphite oxide (GO) to graphene, during which Kapton provided a thermal-stable platform for the reaction [1]. Researchers expected that when GO and Kapton were exposed to lasers, GO would transform into graphene and Kapton into a strong and flexible carbon layer. According to experimental results, graphene and carbonized Kapton formed a compact single layer at the top of the original Kapton film, and the surface could be further processed for a given application. In 2012, a group from UCLA led by El-Kady used a label-printing CD player to produce functional graphene-based sensors on Kapton film by reducing graphite oxide [1]. First, the polymer film was attached uniformly on the unused surface (label side) of the disk. The GO solution was dispensed on the Kapton film in solution form, and solvent was removed by evaporation before further processing. The disk was then loaded into the optical CD drive. Then, the label-writing function of the CD driver and its design software was used to burn patterns of interest onto the disk. This so-called LightScribe function was designed to print labels or covers with photosensitive material for CDs; a pulsed laser leaves a dot on photosensitive paint, and those dots finally form the designed pattern. In El-Kady's research, the group designed desired patterns using LightScribe software and replaced the photosensitive paint by GO covered Kapton film [1] [2]. Due to a weak laser, they resorted to multiple (10-20) passes on a given pattern. According to their experimental results, a large portion of GO successfully transferred into graphene, and performance of laser scribed carbon (LSC) on polymer was close to the electrode produced by high purity graphene, although a large amount of impurities exists in LSC

electrodes [1] [11]. The impact of impurities on the electrical properties was claimed to be minor unless the device was designed to execute high-accuracy chemical or biological analysis. Unlike the conventional approaches, El-Kady's method avoided using pre-made graphene in a separate fabrication process. However, GO ink or graphene paste can become unstable at room temperature or atmosphere. The storage of graphene ink would increase costs, and improper storage would lead to loss of material.

After El-Kady *et al*. published their experiments, Lin *et al*. from Rice University used laser to carbonize Kapton film to obtain graphene-based electrodes [12]. They showed that the LSC layer possesses electrical properties of graphene, and carbonization products of polymer include both graphene and numerous other carbon allotropes existing in the LSC layer. This one-step method significantly reduces the cost and complexity of fabricating graphene-based devices. Although the reaction mechanism of laser induced formation of carbon allotropes on polymer remains unknown [13], researchers believe laser irradiation breaks bonds of organic polymer and forms C=C bonds to produce carbon allotropes. Based on this assumption, academic groups successfully used varied types of lasers to produce graphene-based layers on PVDF and wood in the next few years [14] [15]. Additionally, researchers also designed and developed multiple types of sensors using the laser scribing approach. Compared with high purity graphene, the one-step method produces low-cost devices that demand less in terms of optical properties or mechanical properties from LSC.

2.2 Fabrication of Flexible Electronics

The design and fabrication of partially flexible electronics have already been quite well developed, since PCB is a mature technology. Progress in material science has

provided opportunities to upgrade PCB substrate material as well. In contrast, the design and fabrication of fully flexible electronics demand a much higher amount of material investment and process development. Table 1 shows the existing methods or ongoing research studies which are capable of fabricating fully flexible electronics. Encapsulating liquid or solid metal in a flexible substrate seems to be ideal for flexible electronics, because the carrying substrate and electronics can physically integrate. However, this technique faces numerous challenges, and the fabrication method requires high-accuracy equipment. Furthermore, very few available applications and engineering standards would allow the use and production of Ga-based liquid conductors in electronics.

Table 1: Comparison of important methods to fabricate flexible electronics [16]

	Metal Deposition	Printing			Laser Scribing
		Ink-Jet	Screen-Printing	Roll to Roll (R2R)	
Substrate Material	PDMS	PET, Kapton, etc.			Kapton
Conductive Material	Liquid: Galinstan Solid: Metal	Silver, Carbon Nanotube, Copper, Gold			N/A

Printing has been used to deposit many types of conductive ink on flexible substrates, using techniques that include screen printing, inkjet printing, and roll-to-roll (R2R) processing, both in academic laboratories and industrial contexts [7]. Inkjet printing and screen printing produce reasonably high-resolution products, yet their efficiency is relatively low. They are more qualified for academic use, small-to-medium amount production, or manufacture of high-value products. Ink-jet printing and screen-printing methods have additional operating costs which may be undesirable for devices of average value. Therefore, the R2R process has become a crucial industrial method to

produce large-area electronics on various materials. Nowadays, R2R processing has been generally used to produce flexible versions of flat panel displays, touch screens, and thin film solar panels, due to its extreme efficiency [17]. According to pilot-scale experiments, R2R printing on flexible materials can now reach even micrometer resolution levels in the lab [7]. Hence, with the development of technology, R2R processing will evolve to be much more productive and precise.

Although printing techniques satisfy the demands of flexible electronics markets, some issues cannot be solved using printing techniques. For example, when practicing functionalization on the glossy-finished electrode surface after curing, the compact surface creates numerous technical difficulties for attaching biological molecules on it [19]. Therefore, a one-step fabrication without curing is demanded to satisfy functionalized electronics.

Progress in materials and tool development allows researchers to discover new methods to synthesize, convert, and alter thin films and their surfaces. The laser was utilized to fabricate flexible electronics on organic polymers because its high power induces insulating polymers to transform into a conductive carbon layer. It is an additive technique that does not involve wet processing, cutting, or piercing the substrate. When a well-focused laser scribes the surface in a designed pattern, the surface of the substrate turns into conductor According to the published studies, electrical properties of a laser scribed conductive layer can be very close to the properties of a metallic ink layer on a substrate [16], and the laser carbonization method requires only one step to produce workable devices. Additionally, the conductive layer is a transferred product of the substrate; hence, the contact surface between conductive layer and substrate naturally

merges together. This tight contact contributes to extra strength when devices suffer severe deformation.

2.3 Substrate for Flexible Electronics

Polydimethylsiloxane (PDMS), also known as silicone, is a widely used silicon-based organic polymer. Some of the excellent properties of PDMS cause it to be the ideal substrate material for flexible electronics. At room temperature, PDMS behaves as a viscous liquid, and it transfers into a solid after adding a coupling reagent and baking [16]. Solid PDMS is elastomer, which designates polymers which can be stretched or squeezed when force is applied but which are restored to their original shape when force is removed. The relative permittivity of PDMS is moderate among all organic polymers, and it is non-flammable or non-reactive in air [17]. The fluidic properties of PDMS contribute significantly to encapsulated flexible PCB or liquid circuitry, because liquid PDMS can fit any uneven features on a surface before solidifying. A PDMS replication of the surface can be obtained after liquid fully turns into a solid [17], which is extremely useful in producing low-cost polymer casts or stamps. Biological and medical devices rely on PDMS a great deal due to its high bio-compatibility and chemical inertness. As a result, PDMS is qualified to be an ideal substrate to fabricate electronics. Nevertheless, the price of PDMS is a concern for mass production of flexible electronics. Industrial grade PDMS is priced more than $100 per gallon, and medical grade PDMS is $4,000 per gallon [20].

Theoretically, not only PDMS, but also all insulating non-brittle polymers can be used as substrates of flexible electronics. Although not all commercial plastics have a high structural flexibility and bio-compatibility, they can be extremely low in price. Some

plastic resins even have better electrical properties and thermal stability than PDMS. Hence, a suitable laser modification process would make other polymers, beyond Kapton and PDMS, also applicable to flexible electronics.

Most of the current commercial flexible devices choose polyethylene terephthalate (PET) as a substrate. PET film may be permanently deformed, but the mechanical properties of PET can be maintained at a wider temperature range [21]. The mechanical strength of PDMS changes linearly along with temperature; increasing temperature lowers its elastic constant, and decreasing temperature causes it to become brittle [21]. As for PET, mechanical properties remain stable from -70 ℃ to 150 ℃. PET may cause an allergy for some; hence, the application of PET in wearable and medical devices would be limited. Polyethylene naphthalate (PEN) is another variety of polyethylene family. As compared with PET, PEN resists chemical corrosions more than PET [22]. Moreover, PEN also blocks ultraviolet rays and oxygen from the atmosphere, so it could provide extra protection to circuits or sensors in harsh conditions [21]. Makers of valued flexible electronics prefer using PEN rather than PET in order to extend the device's lifetime. PET is more economical in comparison with both PDMS and PEN; industrial PET sells between $0.1 – $0.2 per kilogram, whereas 0.1 mm thick PEN film in a size of 30 cm * 30 cm is around $200 per sheet [20].

The polyethylene family of polymer is appropriate for mild environmental applications, while more extreme environments require polymers that have a higher dielectric strength or thermal stability. Polyvinylidene difluoride (PVDF) has a high dielectric strength and low biological reactivity [23]. When PVDF forms a copolymer or terpolymer with other organic polymers, it gains piezoelectric and electro-strictive

properties, which make PVDF a good platform to accomplish more complicated tasks [23]. PVDF may cause technical difficulties when printed because the hydrophobic surface reduces the fixation of conductive ink [24]. Kapton is extremely popular and contributes to many applications in the engineering field. It is an orange-yellow polyimide film developed by Dupont. Kapton has the best thermal stability among all commercial polymer, as it retains its mechanical properties from -269℃ to 400 ℃; even if the temperature reaches 480 ℃, heat cannot cause damage to Kapton structure but will only shorten the lifetime of Kapton devices [23] [24].

Table 2 presents the physical data of all mentioned polymers, because they are commonly used as flexible electronics substrates. Young's modulus of each polymer is presented, which is a measure of elasticity of the material; the lower Young's modulus is, the higher the level of elasticity [25]. The properties listed in Table 2 are critical for flexible electronic fabrication, but there could be other requirements as well for a polymer to fulfill in a given task. For example, when designing a single-use flexible device operating in a moderate environment without chemicals, the ideal substrate will be PET due to its low cost and relative chemical inertness. For very harsh, hot, and wet environments, PVDF and Kapton may be a better choice.

Besides polymers, another potential substrate for flexible electronics is paper. Cellulose represents a natural polymer which is synthesized by plants, and it contributes significantly to the composition of paper. In a way, paper can be understood as a natural polymer film. Compared to synthetic polymers, paper offers good absorption, high flexibility, low density, some chemical resistance, and an extremely low cost. According to a study, the cost of paper-based devices can be as low as one cent per piece [8]. Due to

the low unit cost, flexible electronics on paper have the potential to be a single-use multitask device.

Table 2: Comparison of several engineering polymers used for fabrication of flexible

Polymer	Density (g/cm3)	Dielectric constant (25μm, 1kHz)	Working temperature (℃)	Young's modulus (GPa)	Price ($/kg)
PDMS	0.965	2.3	-25 – 200	0.57 – 3.7	4,000
PET	1.380	2.2~3.2	-30 – 150	2.0 – 2.7	0.1 – 0.2
PEN	1.360	3.2	-40 – 160	6.0	15,000
PVDF	1.780	8.4	-45 – 175	1.1	5,000
Kapton	1.420	3.4	-269 - 400	2.5	2,700

2.4 Theory

2.4.1 Carbonization Reaction of Substrate

Carbonization reaction is a general name for a series of reactions which occur either parallel or sequentially. Carbon and its allotropes make up a major proportion of solid products in organic compounds after carbonization. Additionally, the ratio of each carbon allotrope varies when the reactant or reaction conditions vary. Carbonization is distinguished from combustion, because although existing chemical bonds break and new chemical bonds form during both reactions, oxygen or another oxidant must be involved in combustion reactions, yet an oxidant is not essential for carbonization reactions. Moreover, the reaction rate of carbonization and combustion are significantly different; combustion reacts more rapidly than carbonization, the faster reaction rate results in more solid residue remaining after the reaction is complete, and the solid residue is the target

product of the study. Pyrolysis accurately describes carbonization of organic polymers. In a pyrolysis reaction, covalent bonds in reactant molecules break to produce free atoms, and those free atoms eventually form a stable reaction product [13].

Kapton is composited by carbon (C), hydrogen (H), nitrogen (N), and oxygen (O). Figure 4 demonstrates the molecular structure of a Kapton monomer. Once the substrate surface accumulates enough energy from laser irradiation, a pyrolysis reaction will be initiated. The pyrolysis reaction demands a continuous irradiation of lasers to provide reaction energy, because the energy that is released from chemical bonds cracking is unable to maintain the reaction. The overall reaction of Kapton carbonization has been widely acknowledged; Kapton molecules decompose into solid carbon, carbon oxidants, nitrogen oxidants, and vaporized water [26]. Nevertheless, the mechanism for producing carbon allotropes is debatable. Two possible reaction routes are proposed. A laser disassembles Kapton molecules into free atoms, and those atoms arbitrarily combine with each other to form new molecules [26]. Another prediction includes two steps; laser irradiation removes all other elements except carbon by rapid burning, then the laser burning on carbon surfaces produces varied carbon allotropes [27]. Using a laser to burn bulk carbon to produce a mixture of carbon allotropes for further separation is called laser ablation, which represents an industrial method for producing valuable carbon allotropes, such as graphene and fullerene [28]. Figure 4 shows the monomer of Polyvinylidene fluoride (PVDF), another possible material for laser scribe method, which has a similar reaction route from resin to the LSC layer. The pyrolysis reaction of PVDF is similar to the reaction of Kapton, although the molecule structures of two polymers are significantly distinguished.

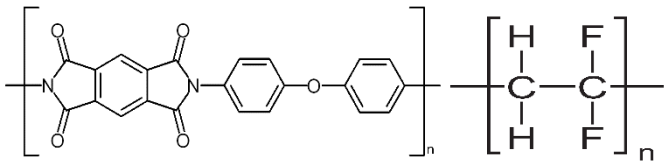

Figure 4. Molecular structure of repeating unit of Kapton (left) and PVDF [29]

2.4.2 Carbon Allotropes

Carbon has multiple forms of allotropes, some of which exist in the natural environment, while some can only be synthesized artificially. Carbon is a vast topic, so this thesis focuses on graphite and graphene due to their outstanding electrical properties as well as their intermediates graphite oxide and graphene oxide. Figure 5 illustrates the structure of three carbon allotropes: graphite, graphene oxide, and graphene. According to the schematic, those allotropes have a carbon sheet structure; carbon sheets are stacked and connected by sp^2 bonds in graphite, and the carbon sheet is independent in graphene oxide and graphene.

Graphite has been used throughout history for thousands of years as a writing or marking material, while in the modern world, graphite has been used as an important electrical material. The chemical activity of graphite is extremely low; even though the contact resistance of graphite is higher than noble metals, graphite electrodes replace noble metals when active chemicals or ions are present in the system. In the next few decades, a marketing increase of lithium-ion batteries will lead to the industrial consumption of graphite, because graphite electrodes are now the sole option for high-performance lithium-ion batteries [28]. Furthermore, graphite can be substituted for noble metal film electrodes in disposable biosensors, because the biocompatibility of graphite is higher and the cost is lower.

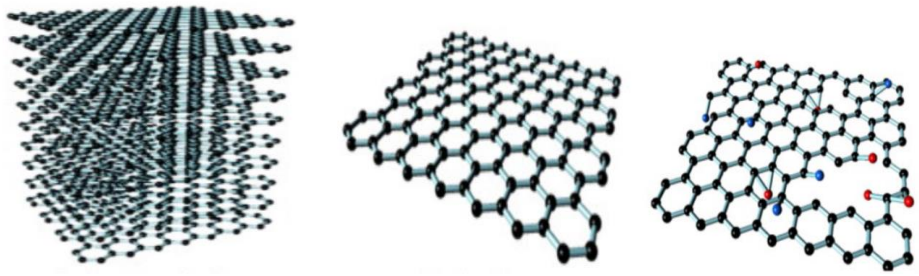

Figure 5. Molecular model of graphite (left), graphene (middle), and graphene oxide (right) [30]

Both graphene oxide and graphite oxide are intermediate compounds; when using graphite to produce graphene, they can be converted easily. Referring to the model of graphene in Figure 5, if oxygen of each graphite oxide layer is intercalated, those oxygen atoms provide van-Der-Waal forces between each layer to sustain the stack structure. Graphite oxide can be obtained by oxidizing graphite with a strong oxidant in an acid solution. Then, ultrasonic exfoliation of graphite oxide is used to form graphene oxide in the solution phase, because van-der-Waal forces are the weakest inter-molecular force. Oppositely, slightly heating or long-time standing of graphene oxide solutions causes reinstatement of van-der-Waals forces, and the graphene oxide solution converts into a graphite oxide solution [30]. Both graphite oxide and graphene oxide have limited application in electronics because of their high resistance; the higher the oxidizing level, the higher the resistance.

Graphene is one of the most promising materials in this century. It is called a super-material by some experts due to its high performance in many fields of applications. Graphene is a two-dimensional material with carbon sp^2 hybridized carbon atoms arranged in a hexagon lattice. It naturally exists in the form of flakes or small

fragments in graphite crumbles [31]. Graphene fragments dispersed in bulk graphite cannot enhance the electrical properties, as graphene only becomes significant when the amount of graphene is large enough. Graphene has notable properties at the molecular level, and researchers generally analyze its quantum phenomena when applying graphene in electronics; however, in the electrical devices tested and examined in this thesis, graphene will be construed as a special carbon allotrope which increases the performance of the devices.

2.4.3 Printing Flexible Electronics vs. LSC Flexible Electronics

Conventional methods for fabricating flexible electronics include inkjet printing and screen printing. Printing techniques have been developed dramatically in the past few decades. Nowadays, ink jet printers are capable of printing high-resolution patterns on various substrates. High-performance inkjet printers dispense ink at 20 kHz frequency, and the resolution is typically limited to ~20microns. In some unique and expensive systems, the resolution can go down to 200 nm, but it can only use specific inks with <10nm particle size. For larger structures, screen-printing is a lower-cost alternative, as the system uses a pre-made pattern in an ultra-fine mesh that can have a resolution less than 50 μm [18] [24] [32].

Industrial inkjet printing or screen-printing are systematic works; the operation concept of both methods consists of depositing a layer of conductive ink on the surface of a flexible substrate. The configuration of printing system is not the sole determining factor, as the quality and composition of conductive ink are even more important. Based on the conductive material, inks can be categorized as nano-metal ink and nano-carbon ink. Those two types of ink are both stable nano-dispersion systems; in such a dispersion

system, surfactants assist metal or carbon nanoparticles suspended in a liquid substrate. Nanoparticle ink is essential to ensure the printing performance and extend the lifetime of printing equipment, because high-resolution printing equipment has extremely small nozzles or mesh sizes. Using nanoparticle ink raises more problems for the storage and post-printing process. Nanoparticles have large surface energy, so an increasing system temperature results in aggregation and sedimentation of nanoparticle ink; coagulation of nanoparticles still occurs along time cumulation even if the nano-dispersion is stored at a low temperature. Therefore, each time before nanoparticle ink is used, ultrasonication and filtration are necessary to ensure ink quality [18].

Conductive ink contains insulating solvents and other chemicals which reduce the conductivity of electrodes; to weaken the negative effect, those inert chemicals must be removed by heating or vacuum vaporization. Heating is used to cure metallic ink, and vacuum vaporization is ideal to cure nano-carbon ink. When placing metal-ink printed devices on a heating source, increasing the temperature vaporizes the solvent, loss of the solvent leads nano-metal particles to conjugate and solidify into a compact film, and the thermal curing of nano-metal ink often takes more than 60 minutes [24]. Vacuum vaporization takes a much longer time to fully cure nano-carbon ink printed devices. Nano-carbon materials such as graphene, fullerene (C60), and carbon nanotube (CNT) become sensitive to oxygen when the temperature is elevated, even though those carbon compounds are chemically inert. As a result, a precise environmental control is critical for curing nano-carbon ink. After the curing and fixation steps, bare printed devices are still fragile, so encapsulation or sealing are recommended to improve mechanical performance and extend the device lifetime.

Nano-metal ink is highly conductive and stable, so it cannot satisfy all working situations. Carbon allotrope ink, especially graphene ink, is promising for sensing, flexible display, and thin film supercapacitors. Printing graphene is a challenging method to deposit graphene on a substrate. In graphene ink, graphene must be in fragment form to fit the printer nozzles or meshes. The excellent properties of graphene cannot be fully exhibited if graphene exists in a fractional form. Improper utilization of graphene ink is considered as a waste of resources. On the one hand, high purity graphene is unnecessary for passive electrical devices such as capacitors or RFID. On the other hand, even some activated devices can use graphene-like electrodes to replace pure graphene electrodes. For those situations, laser scribe carbon (LSC) has the potential to produce low-cost, one-step graphene-content electrodes.

The composition of LSC electrodes on polymer is complex. The majority of LSC is amorphous carbon; although amorphous carbon is conductive, crystallized carbon contributes more to those unique electrical properties. The extremely high price of large graphene sheets limits its application in devices, although it has outstanding properties. Researchers have already examined the possibility of producing graphene-contained LSC layers using an industrial laser to irradiate various materials. The industrial laser irradiates continuously or pulses in engraving or cutting systems, and either the continuous laser or pulsed laser induces carbonization of polymers at the irradiation site. Although there is not a remarkable amount of graphene in the carbonization site, the overlapping of those graphene leaves could provide considerable overall area [33].

Instead of directly fabricating LSC on a flexible substrate, LSC devices can be transferred from bulk material to flexible substrates. A laser was used by researchers

from Rice University to carbonize wood, and the carbonized layer was shown to contain a large amount of graphene [15]. Carbonization was performed on varied wood, which showed the higher cellulose percentage of wood and the higher quantity of graphene contains in the carbonized layer. Then flexible adhesive tape was used to transfer LSC from bulk material to a flexible substrate for characterization and utilization.

The resolution of LSC devices is restricted by beam width, which corresponds to the diameter of a beam. Figure 6 demonstrates how an optical lens focuses a laser beam from a resonator. Ideally, objects are to be placed on a focal plane because the beam has the highest energy density there. A focal plane of lens cannot be adjusted; however, in a laser engraving system, a focal plane can be slightly adjusted by moving the position of the focusing lens. Furthermore, adjusting of the focal plane in laser system is not dynamic; the laser beam must be well focused before fabrication to ensure the quality of LSC devices. Therefore, the laser scribing method is only capable of fabricating two-dimensional devices, and an ultra-flat surface attached horizontally is one of the key factors to guarantee the pass-yield of final product. A high-resolution printer demands more strictness on surface quality, because dust on the printing surface can cause a clogged nozzle due to van-der-Waal forces.

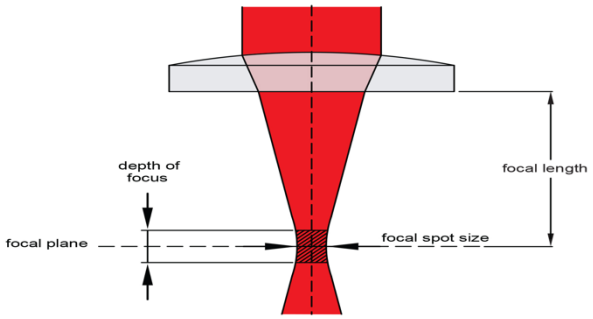

Figure 6. Principle of focusing laser through optical lens [34]

2.4.4 Basic Information of Laser

To fabricate LSC devices, all types of lasers can be used. Based on type of gain medium, all commercial lasers can be categorized into three types: gas laser, solid-state laser, and semiconductor laser (diode laser). Although the gain medium of semiconductor laser is solid, mechanisms and properties of solid-state laser and semiconductor laser are very different; therefore, these two types of lasers belong to different classes. Figure 7 demonstrates the general working principle of gas or solid laser; three major components can be found: energy source (pumping source), laser medium (gain medium), and optical resonator, which is constructed by one fully reflective mirror and a partially reflective mirror. Electrons in medium transit from low energy level to high energy level when external energy is applied, photons are released during the process, and light is reinforced in the resonance cavity by multiple reflections until the light beam is strong enough to travel through the partially reflective mirror. Varying mediums of laser generators will result in laser possessing different wavelengths, and the illustrative behavior of different wavelengths of laser is identical in color. A CO_2 laser plays a critical role in industrial areas due to its high power and high efficiency. The wavelength of CO_2 laser varies from 9,400 nm to 10,600 nm, and electromagnetic waves in this spectrum range are red and infrared.

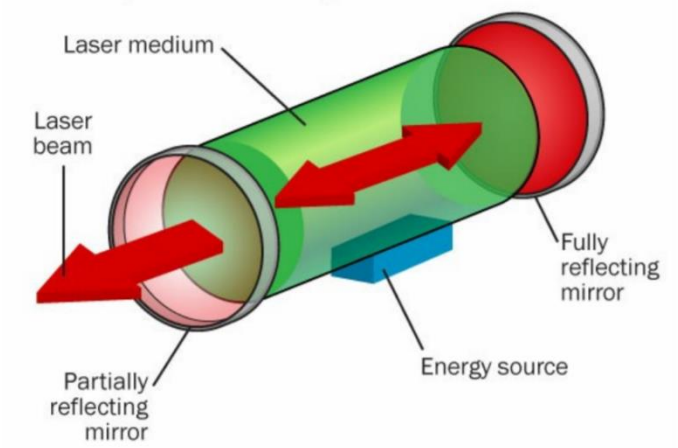

Figure 7. General structure of solid-state laser generator [35]

Semiconductor laser contributes more in everyday life because most semiconductor laser diodes emit visible light (λ=380-750 nm); although the wavelength of semiconductor laser covers from 374nm - 3500nm, industries do not utilize laser diodes as much because catastrophic optical damage occurs only in high power operations. A semiconductor laser diode has a similar structure to a solid-state laser generator, as shown in Figure 6, but the medium of semiconductor laser diodes is not made by a single type of material. Semiconductor laser diodes have a piece of n-type semiconductor and a piece of p-type semiconductor mounted parallel to each other but perpendicular to reflective mirrors. The surface between p-type semiconductor and n-type semiconductor, called p-n junction, is the activate location where photons emit.

2.4.5 Three-Electrode Cyclic Voltammetry

Cyclic voltammetry is a common and reliable electrochemical characterization method, and the measurement is also sensitive to trace amount of target chemicals in an electrolyte solution. Figure 8 illustrates the majority components of a three-electrode chemical cell: the working electrode (WE), counter electrode (CE), and reference electrode (RE) are fully immersed in electrolytes; voltage and current is measured

between WE and CE. Then, a C-V curve based on the correlation between voltage and current is plotted for analytical purposes.

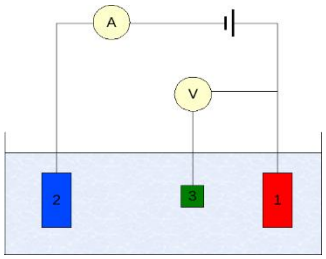

Figure 8. Setup of three-electrode cyclic voltammetry cell

(1) Working electrode (2) Counter electrode (3) Reference electrode [36]

In the cyclic-voltammetry technique, the cell is driven by a voltage which is changed linearly over time applied between WE and CE; when the voltage reaches the set point, the applied voltage drops back to its initial value at same rate. A reversible reduction-oxidation reaction of analyte occurs on surface of WE and CE, respectively, because of electrons' flow. When electrons flow from WE to CE, oxidation happens on WE surface and reduction happens on CE surface; when electrons flow oppositely, reduction happens on WE surface and reduction happens on CE surface. Voltage between WE and CE impacts the level of reduction-oxidation reaction, and those reactions cause a concentration change of oxidation or reduction products on the electrode surface. Therefore, current change, which is correlated to voltage change, is observed because chemical concentration determines the conductivity of solution. The concentration of the analyte determines the height of the peak in a C-V curve; moreover, the position of the peak is distinguished from chemicals due to a different bond energy and resistivity of each chemical.

2.5 Laser Engraving System

The premise of this research is to explore not only the laser scribe process, but also entertain the possibility that it can be done with very basic and low-cost instruments. As a matter of fact, laser writing, engraving, and cutting tools have become more capable while decreasing in cost in the recent two decades, thanks to low-cost digital controllers, solid-state lasers, and increased interest from the hobby community that opens up a market for large scale production. Therefore, in this work we utilized a low-cost system acquired from Amazon Marketplace to initiate our project.

Figure 9 shows the elements of the low-cost laser engraving system used in this thesis. The laser head is mounted to a stage which is driven by two step motors, and those motors enable the laser head to move in a horizontal plane which is parallel to the working surface. The distance from the laser head to the working area is fixed; in addition to this, the focus of the laser has to be accomplished manually every time before the engraving process, unless the substrate is the same as the previous working trail. The laser head can be replaced by a user to adapt to different tasks; a square ware which has a frequency of 1 kHz and an amplitude of 12 Volts will comes from the controller board and power up the laser head.

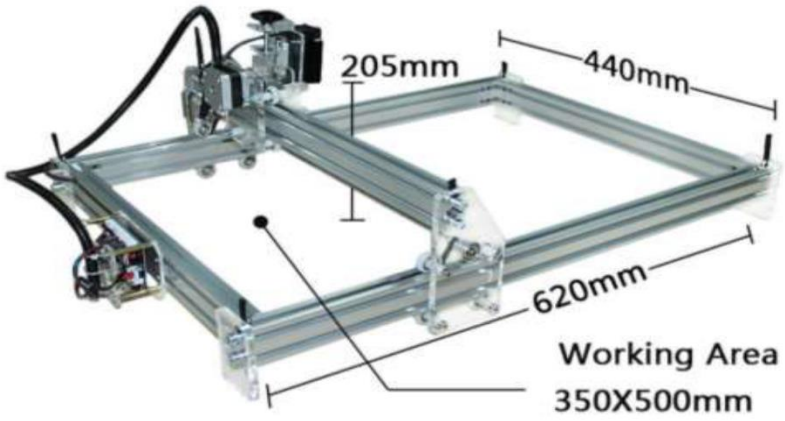

Figure 9. An overview of laser engraver used in the study

The system is driven by G-code based software provided by the manufacturer. Three operational parameters can be changed through the user's interface: power level of laser head, engraving speed, and line density. The engraving speed represents the movement speed of the laser head along the shorter side of the working area during the engraving process. The movement of the laser head in the short side direction is more precise than movement in the long side direction, because the short side movement is driven by a set of gears and a belt, while the long side movement is only driven by a belt. A remarkable amount of heat would be generated and accumulated in a laser diode while the laser head works, so efficient cooling is the key factor to determine the performance of a laser system. In this system, two cooling methods are performed; the aluminum case of the laser head is a heat sink which is capable of removing heat from the laser diode, and an external cooling fan is mounted to the upper end of the laser head. Even though heat can be removed in two methods from the laser diode, the cooling rate still cannot satisfy continuous, long-time utilization. The manual recommends that users allow the system to fully cool down for thirty minutes for every thirty minutes' usage to extend the lifetime of the laser.

2.6 Applications

2.6.1 Super capacitor

A supercapacitor is a type of passive electrical device which can be made with graphene; a graphene-based supercapacitor has a lower manufacturing cost and higher electrical performance [31]. The electrostatic double-layer capacitor (EDLC) currently utilizes activate carbon electrodes due to its large surface area, but the conductivity of activate carbon is not ideal [33]. Replacing activated carbon by graphene significantly increases the conductivity of the electrode, while meanwhile, the graphene electrode enlarges capacitance and energy density by providing more surface area [33].

2.6.2 Sensors

Carbon-electrode devices are capable of replacing noble-metal-electrode devices for electrochemical analysis when halogen ions are present in the system, because halogen ions and noble metals form water-soluble coordination complexes [37]. Moreover, a carbon electrode is an ideal biological sensor because of its high biocompatibility; several types of flexible biosensors can be made with carbon material, for example, strain/flexibility sensors and electrochemical sensors. Furthermore, based on the working principle, an electrochemical sensor can be further classified as a voltammetry sensor, resistance sensor, and field-effect-transistor (FET) sensor [5] [8]. Chemical or biological sensing is performed in a complicated environment which has a lot of background noise, and voltammetry sensors and resistance sensors are less selective or sensitive in such a complicated environment; therefore, FET, which has a modified electrode surface. is more suitable for this situation. The gate surface of modified FET is attached by chemicals or cells which are highly selective to target

analyte, and a signal would be observed as soon as binding or reaction happened on the gate surface [8].

Conventional FET is made by semiconductor material, so chemicals or live cells are difficult to attach to the surface. A graphene membrane could be desired gate material to fabricate flexible modified FET sensors, because graphene is the most pliable but strongest material [30]. In addition to this, the net structure of graphene provides an efficient capture site for chemical or biological reagents. Figure 10 demonstrates the design concept of a functionalized graphene membrane for biological sensing [37]. The functionalized membrane is attached to the gate of FET by functional molecules; when the target molecules are bound to the functional molecules on graphene membranes, change of gate will result a current change through FET.

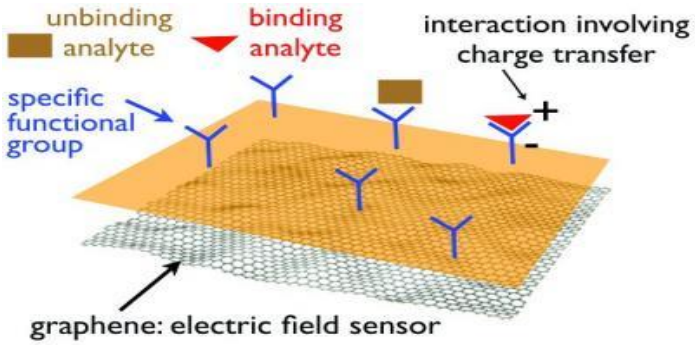

Figure 10. Schematic of modified graphene gate on field effect transistor (FET)

CHAPTER 3: ENGRAVING OPTIMIZATION

The laser engraving system has three variable parameters: the power output of a laser, the engraving speed of a laser head, and the density of lines. The tuning range for each parameter is 0 – 2 Watt, 200-2000 mm/min, and 10-20 lines/mm, respectively. Those three parameters will affect the unit energy delivered to the surface by the laser. Although more environmental parameters can be modified in the carbonization process, such as ambient gas and temperatures that can significantly change the pyrolysis reaction and the resulting ratio of carbon allotropes, those parameters will not be examined at this time. This would require a more expensive setup, and vacuum operations are not possible at this time. Consequently, this chapter will investigate how laser doses delivered to the surface affect the properties of carbon allotropes layers. Furthermore, optimal parameters that are capable of producing the least resistant carbon layer on a substrate will be established.

3.1 Carbonation Test on Various Material

Previous researchers examined LSC fabrication on Polyimide (Kapton), PVDF, and wood. Additionally, the laser tools used in those studies varied from a 45W CO_2 infrared laser to a 15W violet diode laser. Whereas the only available laser tool in the lab is a low power (P_{max}=2.5W) blue-violet laser (λ=445nm, Appendix A presents the spectrum measurement of the laser used in this study), carbonization tests were initially performed on various flexible materials to verify the possibility of a viable reaction. Figure 11 shows the carbonization result of various materials. The output power of the laser was tuned to max, and the test area was restricted to a 10×10 mm area on each material. Kapton film and paper were obtained from a commercial supplier, but PVDF

was fabricated in the lab. The PVDF solution was prepared by dissolving it in dimethyl sulfoxide (DMSO), then spin-coating the solution on glass slides with a speed of 800 rev/min provided approximately a 0.3 mm thickness film for further experiments.

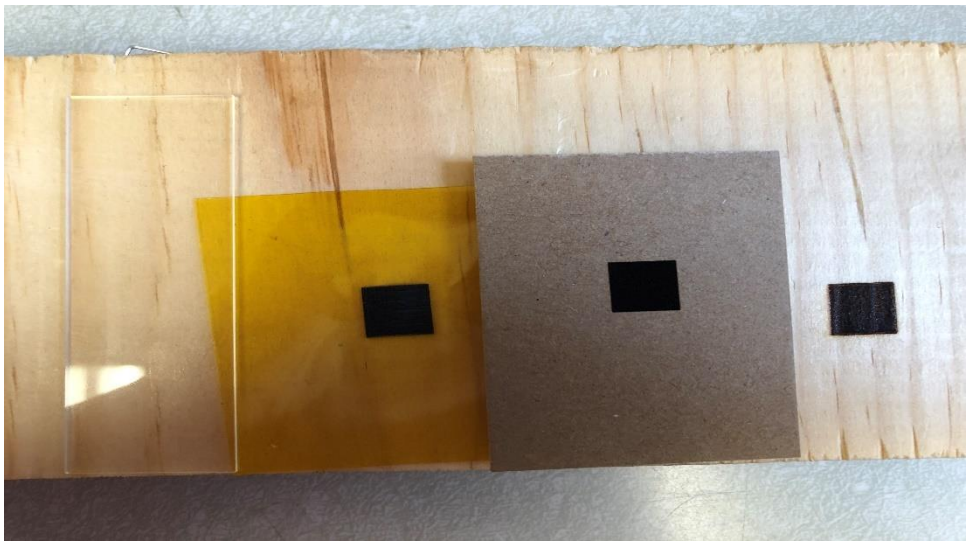

Figure 11. Carbonization tests on PVDF, Kapton, cardboard, and cedar wood (from left to right)

Our preliminary experiments indicated that polyimide (Kapton®), wood (Cedar, *Idoha Timber LLC*.) and paper could be carbonized when the output of the laser system was maximized. Deformation and curling of the substrate were observed at the edges of the carbonization area on Kapton film, due to the thermal shrinkage of the Polyethylene terephthalate (PET) support layer underneath. Commercial Kapton films are commonly attached to a thicker PET substrate to prevent bending damage and ease of handling. The Kapton films used in this study had thickness of 0.12 mm, and each of the films was attached to a 0.5 mm thick PET. In addition to thermal shrinking, partial melting and burning also occurred on the PET backbone. The literature shows that Kapton remains

chemically stable at more than 400 ℃, yet PET has a glass transition temperature (T_g) of 67 ℃, which is much lower than the temperature at the laser irradiated region. Accordingly, the PET backbone was removed, and bare Kapton films were temporally attached to a thermally-stable substrate to retain the flatness of Kapton during the laser engraving process. Figure 12 shows Kapton film attached on glass slides; this configuration allowed Kapton to receive a higher laser irradiation than thermal limitation of PET. This is because the glass support layer has a higher thermal capacity and thermal conductivity than PET, and hence is more efficient in removing excess heat from the surface.

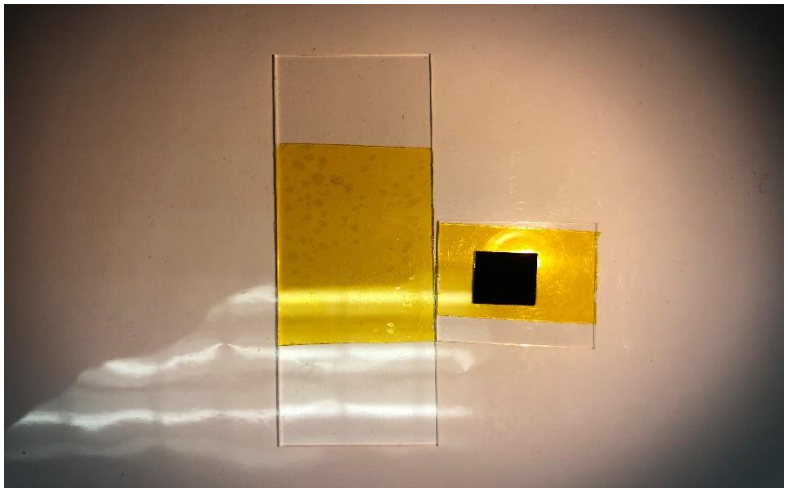

Figure 12. Kapton film on glass slide. Carbonized Kapton (right) remains flat compare with unreacted Kapton (left)

We also attempted to carbonize other organic media using the laser engraver. The relatively low-power laser showed it is capable of carbonizing hard wood (cedar) material as well (Fig.11). Nevertheless, growth rings of wood result in uneven density of material, and the carbonization level varies across the surface. Further studies are needed to

establish an optimized writing method that reduces the growth-ring effect to a minimum. In contrast, standard thin office printer paper burned dramatically faster when irradiated with the laser, making the carbonization process hard to control. As compared to printer paper (Biose® X-9® Multi-Use Copy Paper), a high-density paperboard (used commonly in mail packages and also known as chipboard) shows lower inflammability under laser irradiation. Cellulose fibers in paperboard are packed in denser form, and most of the paperboard contains inert material to increase its mechanical strength. Therefore, paperboard tolerates more laser irradiation, and the denser cellulose pack provides a finer carbon layer at the top.

Although PVDF film showed insignificant color change after laser irradiation, a multimeter measurement indicated that the film remained insulating. A slight discoloration indicated that PVDF absorption was insufficient for an adequate level of carbonization. Dissimilar optical properties of PVDF and Kapton led to the different laser irradiation results. Figure 13 plots the transmission spectrum of PVDF and Kapton; PVDF shows high transparency to visible light, yet Kapton absorbs a large amount of visible light that has a wavelength between 400 nm to 500 nm. The wavelength of the laser used in this research is 445 nm, which falls into the absorption spectrum of Kapton. The energy carried by the laser is absorbed less efficiently by PVDF, and a pyrolysis reaction cannot be triggered. As a result, Kapton was the sole polymer material used in the research, while wood and cardboard would be further compared in the following series of experiments. Appendix B performs calculation of energy threshold to carbonize polyimide and cardboard.

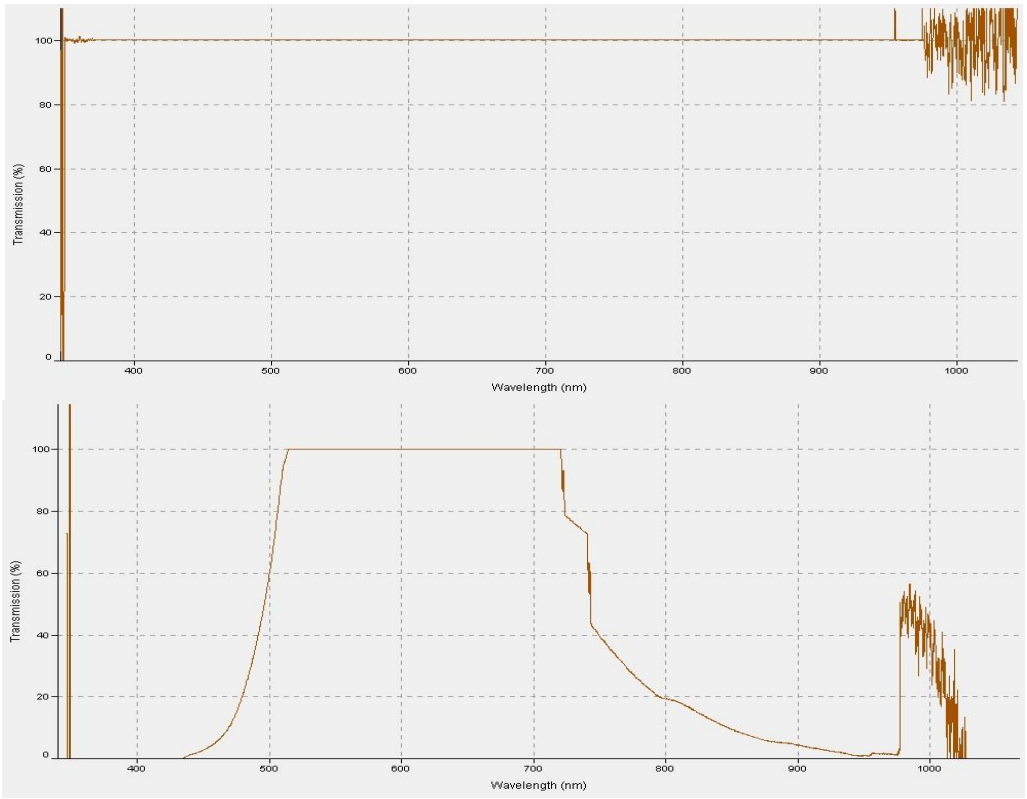

Figure 13. Transmission spectrum of PVDF (top) and Kapton (bottom) in wavelength range of 350 nm to 1000 nm

3.2 Parameters Impacting Laser Dose

Carbonization of a substrate is initialized by the accumulated energy of a laser on the surface; a higher dose of laser should lead to a higher rate of energy accumulation. For the engraving system used in this work, three factors determined the laser dose: power of the laser beam, engraving speed, and vertical line density. The laser irradiates at a constant frequency of 1kHz, and the diameter of laser beam is ~0.5 mm when the beam is focused correctly. Pulse width modulation at the controller determines the intensity of the laser beam; a higher intensity beam has a longer pulse duration. A stationary laser beam burns a ~1 mm diameter single carbon dot. When the laser head moves, such

carbonized dots construct a line pattern. Thus, the density of carbonization dots is directly proportional to the engraving speed. So, at low speeds, high dot density results in a excessive amount of burning through the substrate material. Yet, at very high speeds, insufficient dot density leads to gaps in the carbon layer that reduces the conductivity. In addition, line density (number of lines per millimeter of a filled area) can vary from 10 to 20 lines/mm via the software driver. This perpendicular line density has similar properties as dot density, and its optimal choice can play an important role in the performance of the final product.

3.3 Optimization of Laser Writing Process

The previous chapter showed that one of the major applications of laser-induced graphene (LSC) is to form conducting electrodes/tracks in flexible electronics, for which sheet resistance is the key factor of performance. The previous section listed multiple process parameters that influence the composition of LSC on a given substrate. In this section, the outcome of series of experiments that examined the impact of these operational factors on conductivity of LSC on various flexible materials are presented. Moreover, the optimal operational parameters responsible for the lowest sheet resistance are to be determined, which will then be used to fabricate functional devices.

Two types of resistive elements were fabricated to test the influence of process parameters on LSC performance on Kapton and cellulose products. Figure 14 are pictures of a Van der Pauw (VdP) test structure and linear resistor fabricated on Kapton using a laser engraving system; the VdP pattern, which is used to determine sheet resistance in a four-probe measurement, has dimensions of 10mm ×10 mm and four corner contacts with

1mm overlap, and the linear resistor has dimensions of 3 mm in width and 20 mm in length.

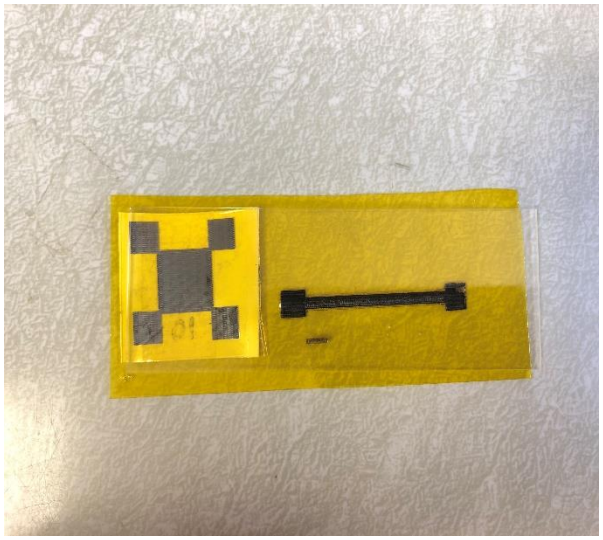

Figure 14. Van der Pauw structure (left) and linear resistor (right) on Kapton film

3.3.1 Variation in Laser Power

LSC resistors on Kapton film were fabricated using various power levels, while linear writing speed and line density were fixed. The power of the laser was modified through the user interface from 20 Unit (refer Appendix B for power conversion between unit power and power in watt) to 100U in 5U steps. Plots in Figure 15 present the changing value of resistance as power increases. Laser power below 20U was incapable of triggering carbonization reaction on Kapton film. Resistance of LSC initially decreased along with the increasing laser power. Resistance of LSC layer reached the lowest point around 70U, after which a higher power could still increase the carbonization level or type of Kapton without further resistance dropping. In some experiments, high power produced resistors were occasionally as low as 12 Ohm/cm^2, which had very poor stability or reliability, as such a large dose caused frequent burn through the entire Kapton film. Pictures in Figures 16 show the back and front of laser-

damaged Kapton films when a laser operated at maximum power, where clear twisting and deformation are visible. Moreover, a large amount of bubbles can be observed between Kapton film and PET substrate. Those bubbles reduce the structural strength of the LSC layer, and any minor movement or vibration causes the LSC layer to exfoliate from the substrate.

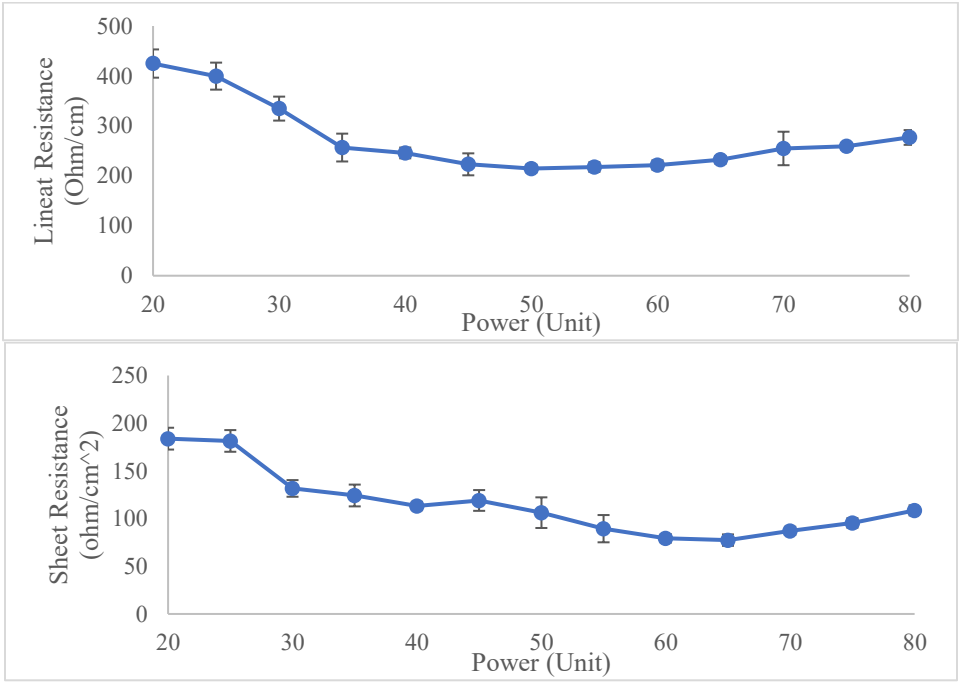

Figure 15. Changing of linear resistance (top) and sheet resistance (bottom) of laser scribed carbon (LSC) on Kapton film over laser power

It is also notable that the surface of LSC generated by a high power laser is rougher. The comparison in Figure 17 presents 50x-magnified pictures of the LSC surface on Kapton written with a 100U laser and a 50U laser at same engraving speed, respectively. A LSC formed by a low power laser has a more uniform and glossier surface. A flat and glossy surface is fundamental to the performance of electrodes used in

electrochemical cells that are capable of a shorter response time and higher accuracy for analysis.

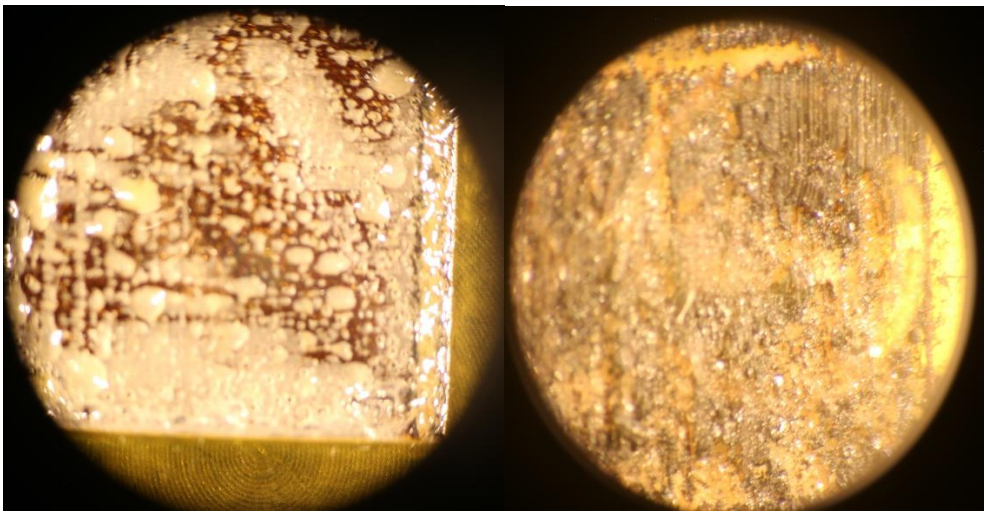

Figure 16. Changing of linear resistance (top) and sheet resistance (bottom) of laser scribed carbon (LSC) on Kapton film over laser power

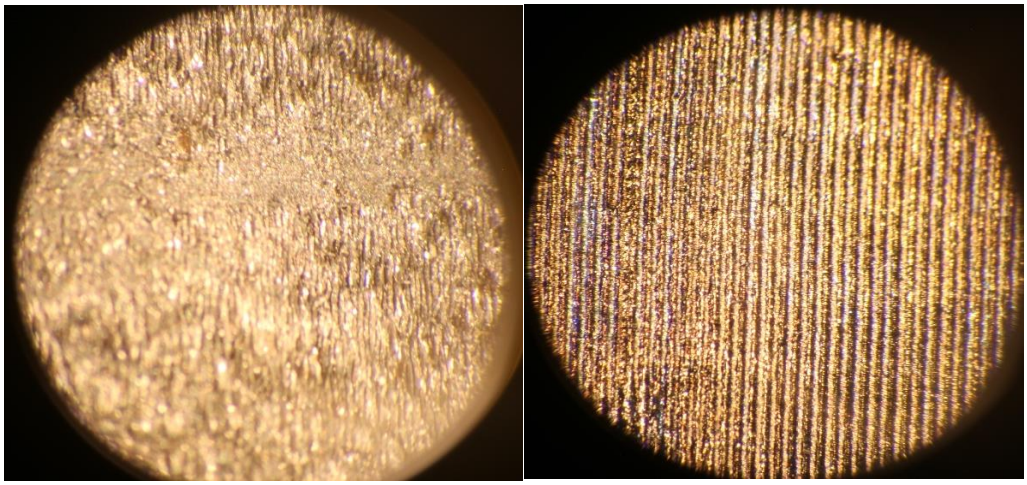

Figure 17. Surface of LSC carbonizing with high dose laser (left) and low dose laser (right) under 100X microscope.

3.3.2 Variation in Engraving Speed

Engraving speed has a similar influence on LSC conductivity as laser power. However, the influence of engraving speed is more remarkable. When laser power and line density remain constant, a slower engraving speed creates larger overlaps between each individual carbonized dot. The results in Figure 18 indicate that the largest conductivity in the LSC layer appears for a linear speed between 800 and 1200 mm/min. Microscope observation proves that a very slow engraving speed induces substrate damage, which is highly similar to the high laser power damage presented in Figure 16. Engraving speeds larger than 1200 mm/min induce incomplete carbonization of the substrate surface. The electrode surface in Figure 19 represents an uncompleted carbonized Kapton; the LSC layer is comprised of a large amount of polymer residue which increases the resistivity of the LSC layer.

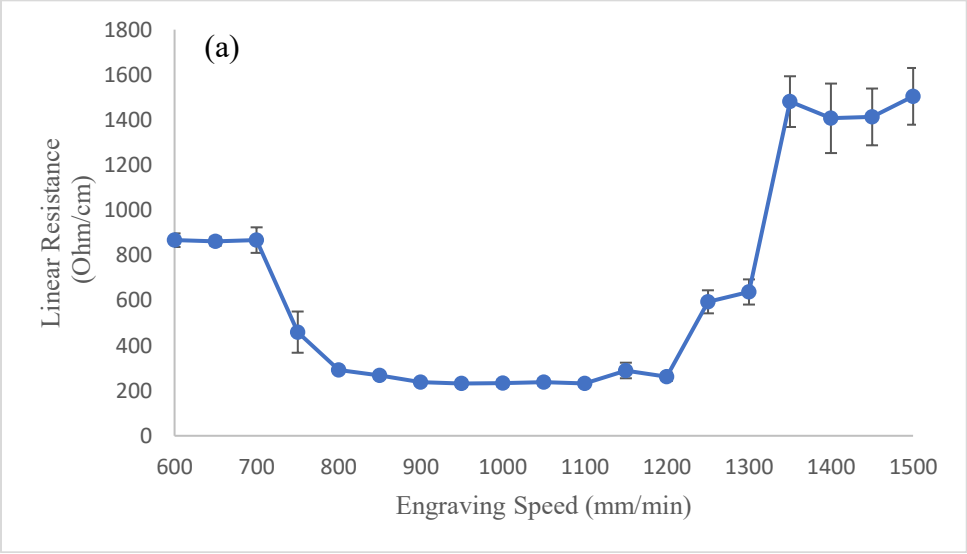

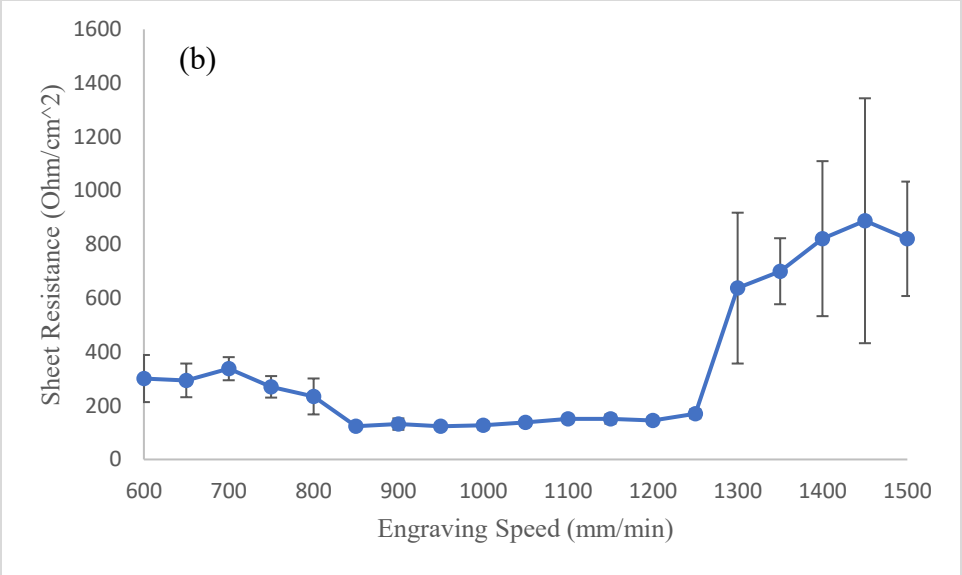

Figure 18. Changing of linear resistance (a) and sheet resistance (b) of laser scribed carbon (LSC) on Kapton film over engraving speed

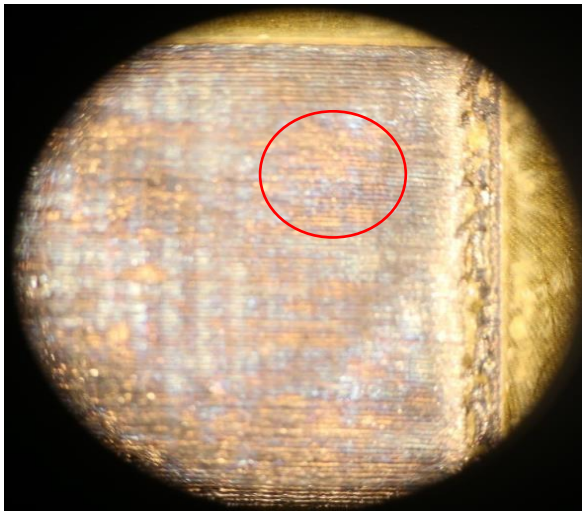

Figure 19. Incomplete carbonized surface caused by high engraving speed (1500 mm/min). Yellow color in circle represent uncarbonized polymer

3.3.3 Variation in Line Density

According to the plot of line density vs. resistance in Figure 20, line density seems to be a minor factor which influences the performance of the conductive LSC layer on Kapton. Varying the line density at a constant laser power and engraving speed results in only a 15% drop in LSC sheet resistance. Since the diameter of the laser beam is 1 mm, a line density of 10 lines/mm should exactly fill the location. Denser lines may lead to repeating carbonization at the same location, however, no heat damage could be observed when line density was double the initial density. In the engraving system, designed patterns were finished line by line, and the laser head would not return to the same location until it burned a continuous line. Hence, a given carbonized zone has that traveling time to cool down and release part of the accumulated energy, which helps the substrate survive from high line density. We should also remember that an actual laser beam has a radial Gaussian profile, hence only the very center ~0.3mm is truly exposed in each dot, and pulses do not exactly emerge side by side in adjacent lines. Moreover, the current window of 10-20 lines/mm is imposed by the software driver, and clearly going substantially beyond these extremes will lead to either no overlap (high resistance) or excessive overlap (heat damage, hence high resistance) that only shows as a 15% increase at either extreme of Figure 20. As such, the optimal line density appears to be between 15 and 17 lines/mm.

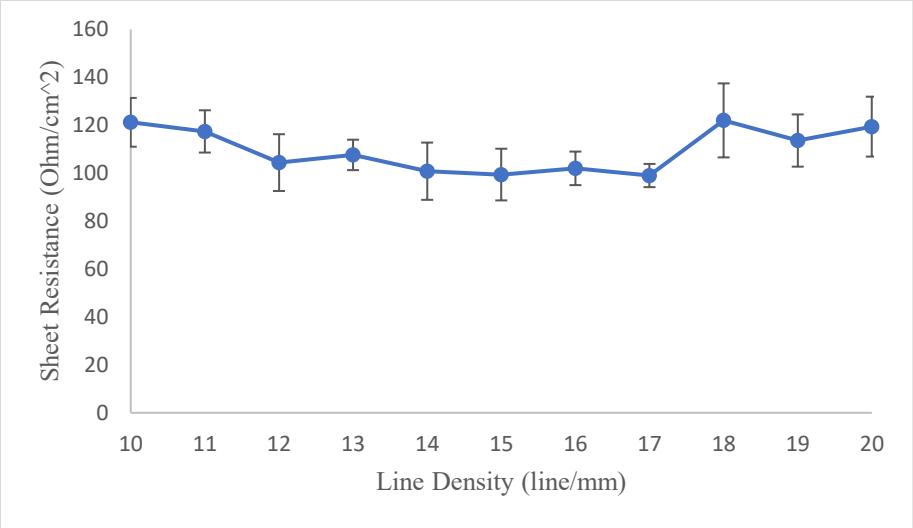

Figure 20. Changing of sheet resistance of laser scribed carbon (LSC) on Kapton film vs line density in line/mm

Measurements obtained from the Dektak-2 profilometer in Table 3 express the relationship of total post-carbonization thickness and laser power. Total post-carbonization thickness includes the thickness of the LSC layer and substrate after carbonization process was finished. Commercial Kapton film commonly has a thickness less than 0.2 mm, and the increase of thickness is much larger compared with the original thickness. In this experiment, LSC layer conjugates tightly with the remaining Kapton, which is fragile due to the minute thickness. The available tools in the lab could not exfoliate the LSC layer without damaging the unreacted Kapton; therefore, the total post-carbonization thickness was studied instead of the actual thickness of the LSC layer. According to the data, the increase of thickness is not relative to the laser dose base on the result of 4 different power levels.

Table 3: Thickness measurement of carbonized Kapton fabricated using different power level

Trail number	Increased thickness (mm) at different power level			
	30 Unit	50 Unit	70 Unit	90 Unit
1	+0.089	+0.088	+0.083	+0.080
2	+0.079	+0.080	+0.085	+0.081
3	+0.081	+0.086	+0.084	+0.079
4	+0.085	+0.088	+0.093	+0.084
5	+0.088	+0.076	+0.080	+0.092
Average	+0.084	+0.083	+0.085	+0.083

The scanning electron microscope (SEM) image in Figure 21 proves the change of microstructure of Kapton. Given that a pulsed laser induces a very uneven heat distribution and many forms of carbon allotropes are to be found in the irradiated polymer, the resulting surface is complex. The carbonized layer includes structures that intertwine with each other to form a very porous carbonized polymer film as the resulting gas phase byproducts produced during laser-induced pyrolysis reaction escape. Pores in the structure offer opportunities for chemical or biological sensing; meanwhile they may also impair the mechanical strength of the LSC layer. The lower-resolution picture clearly demonstrates the presence of dense carbon plates induced by a pulsating laser, and the 10 μm resolution picture shows the porous structure of carbon with a given thicker carbon platelet. The size of platelets seems non-relative to the laser dose and more associated with the pulse duration and line speed, and it remains unknown how the grain size contributes to the electrical properties of LSC layer in a specific way.

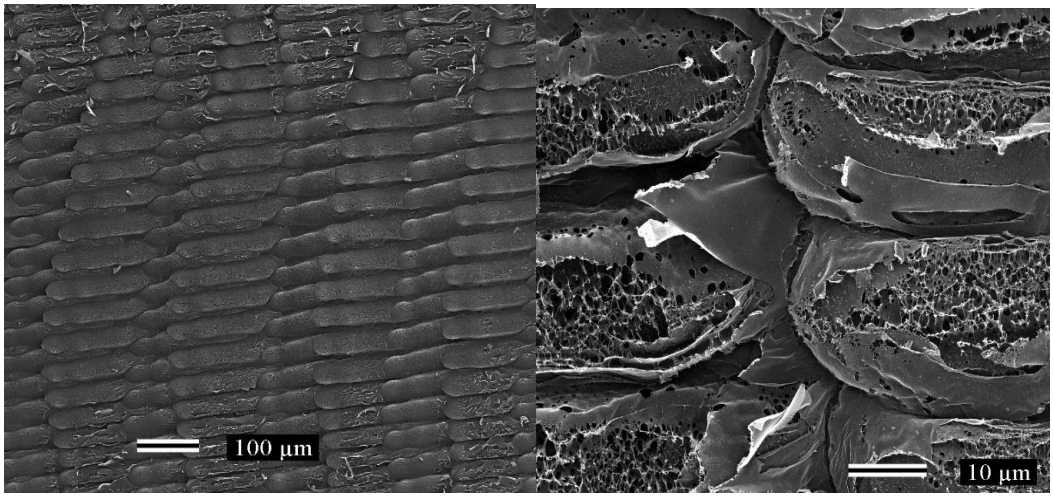

Figure 21. Scanning electron microscope (SEM) picture of carbonized Kapton

Table 4: Optimal parameters to fabricate least electrical resistant LSC layer on Kapton

Power Level (unit)	50 – 60
Engraving Speed (mm/min)	900 – 1100
Line Density (line/mm)	16 – 17

Based on the systematic study above, the optimized operational parameters for producing a highly conductive electrode on Kapton are listed in Table 4. The exact operational parameters may be varied in the listed range and the quality of the resulting LSC layer may still depend on the overall thickness of Kapton film and backbone substrate. Thicker films or Kapton films on glass tolerate a higher laser dose as compared to PET-supported Kapton. Fine features should be fabricated using a lower laser dose and moderate speeds, because high intensity irradiation accelerates the pyrolysis reaction and excessive and rapidly produced gas byproducts result in coarse edges and uneven surfaces. Exfoliation of the LSC layer has not been observed in experiments; however, cracked LSC surfaces are occasionally observed at a relatively high-power engraving. Repeated tests indicate LSC only cracks if Kapton films are exposed to the atmosphere

for a long time, as Kapton is capable of absorbing water up to 2.8 % of its own weight from the atmosphere at equilibrium [16]. During a high-power operation, initial carbonization happens quickly on the surface and further carbonization deeper in the film evaporates the water absorbed by Kapton, rapid evaporation of which causes severe expansion inside the LSC layer. Figure 22 shows a cracked surface of LSC which is fabricated on a Kapton film that had been exposed to the atmosphere over thirty days; after two hours baking at 60℃ in a vacuum oven, cracks could not be observed on the LSC fabricated on the same Kapton film. Vacuum baking is necessary for “aged” Kapton films, so we can remove excess water content of Kapton to ensure the quality of the LSC layer.

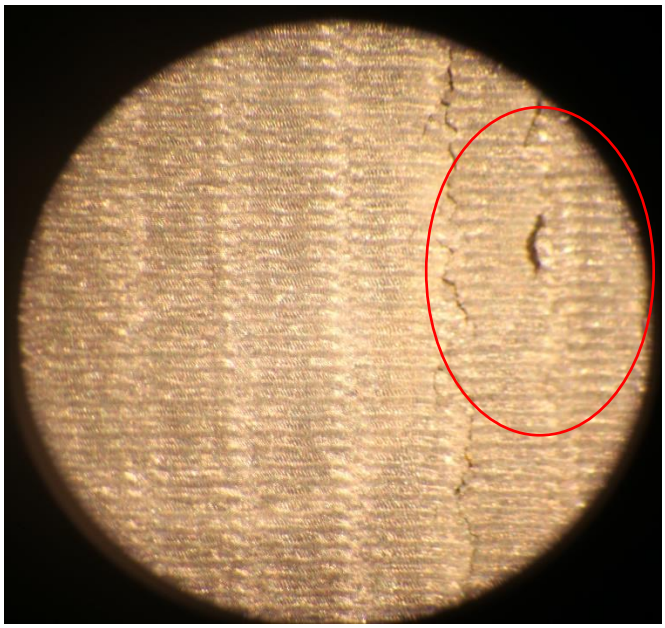

Figure 22. LSC layer on aged Kapton. Similar cracked could be observed at random location on the LSC surface.

3.4 Optimized Carbonization on Cellulose-Based Material

Cellulose-based materials considered in this study include cedar wood and cardboard, which display a similar performance response to the operational factors of a laser system as Kapton. Firstly, a high laser dose reduces resistance by increasing the carbonization level. However, laser induced heat damage to the substrate does not occur on wood or cardboard. Resistance of LSC keeps decreasing when the laser dose increases, albeit with a slower rate after 60U. Figure 23 illustrates the correlation between laser power and sheet resistance as well as the final LSC thickness on cardboard. According to this data, resistance decrease tends to be minimal when laser power is greater than 70U. Meanwhile, the measured LSC thickness on carboard indicates that a LSC layer stops growing when laser power is greater than 60U. Optical spectra of the resulting LSC layers (not shown here) proved that it absorbs large (+95%) amount of incoming light in a wide spectrum. Therefore, along the growth of the porous LSC layer, a laser beam is fully absorbed and decays in this layer. No further carbonization occurs due to strong absorbance, and the thickness of the LSC layer remains constant beyond a limit.

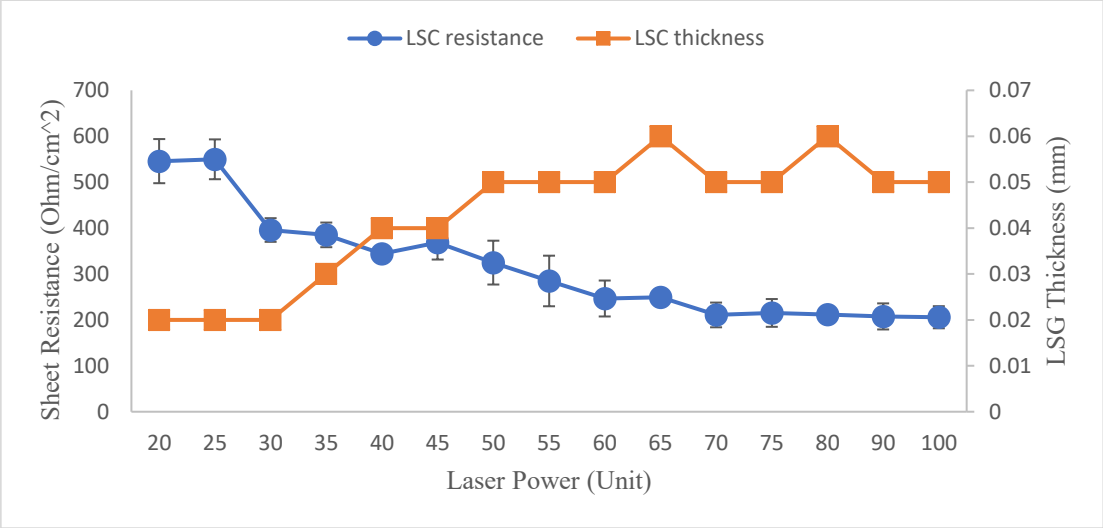

Figure 23. Resistance and thickness of LSC layer change over laser power on cardboard

Line writing speed is an important parameter for the LSC on cardboard. Above an engraving speed of ~1200 mm/min, there remains a significant amount of uncarbonized cellulose fiber in LSC layer, and the resistance of some LSC samples fabricated with fast engraving speeds (>1500 mm/min) reached 2500 ohm/cm^2. Cardboard and wood have less flexibility and may not be easy to apply in some applications. Thus, it is best to transfer the LSC layer on the cellulose material to a truly flexible substrate such as polymer or paper. For instance, adhesive tape can remove a LSC layer from cardboard or wood after the substrate has cooled to room temperature. The orange points in Figure 24 represent resistance measurements of the LSC layer after it is transferred using this adhesive tape. Sufficiently thick LSC provides a uniformly transformed LSC film on tape, and the resistances of on-substrate film and transferred film have an insignificant difference. High engraving speed reduces the amount of LSC on the surface, and transferred film becomes non-conductive due to the discontinuity of carbon on the film. Line density between 600 and 1100 mm/min also has a minor influence on the conductivity of LSC on cellulose material.

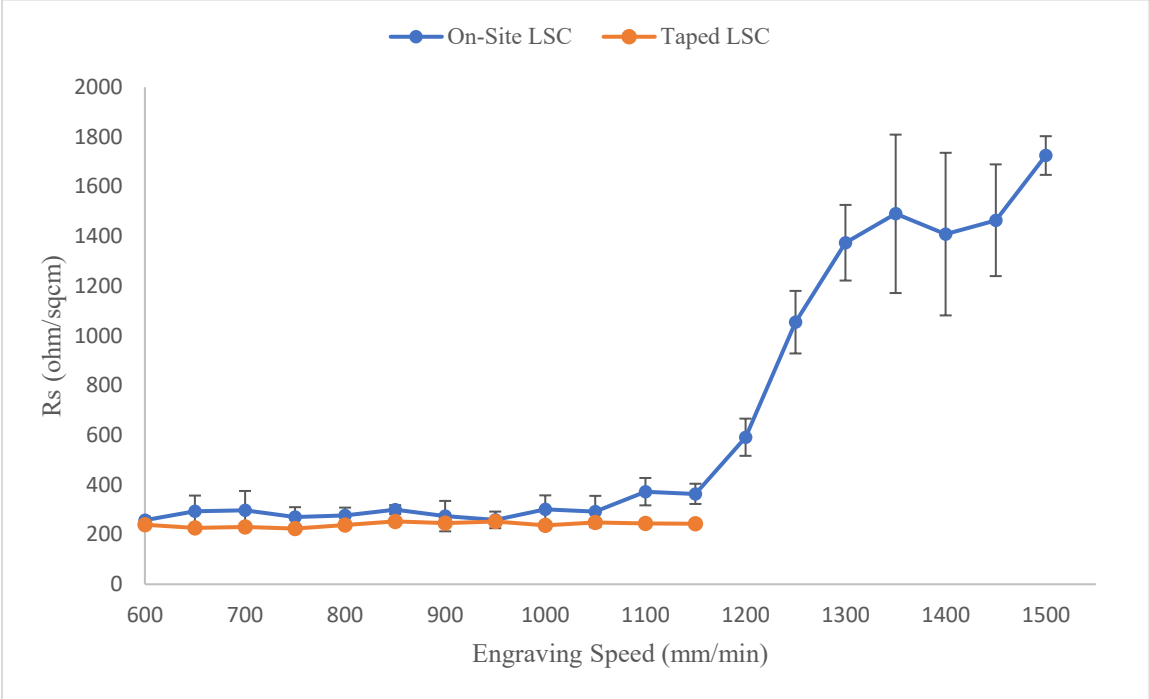

Figure 24. Resistance and thickness of LSC layer change over engraving speed on cardboard

3.5 Composition Analysis of Carbon Allotropes

A LSC layer on either Kapton or cellulose contains various carbon allotropes as discussed in the previous chapter, with a distinct crystal structure of each allotrope. The proportion of carbon allotropes determines the overall properties and application of carbonized electrode. In this study, Raman spectroscopy was used to distinguish the allotropes found in the final LSC layer. The Raman shift is considered to be a fingerprint of a given material because it is determined by the nature of molecular bonds and crystal structure. Figure 25 show a library of example spectra that illustrate Raman shifts of 3-D carbon allotropes, graphene oxide, and graphene. Raman Shift signals of those allotropes generally occur at a narrow wavelength region; however, the number and strength of

overlapping peaks may vary at specific wavelengths. Such overlaps also result in inaccuracy in quantitatively analyzing the ratio of the contributions from different types of allotropes with large similarities in crystal and bond structure. Professional analytical software capable of associating overlapping peaks to specific structures in different ratios is needed to deliver accurate results. We refrained from doing so in this study for three reasons: a) Our laser and its driver do not have independent control of pulse amplitude and width, two parameters needed for a highly-controlled process that can alter everything; b) all carbon allotropes are already identified in the LSC layer according to published research [38]; and c) the existence of multiple allotropes is a point of strength in sensor applications and not a threat.

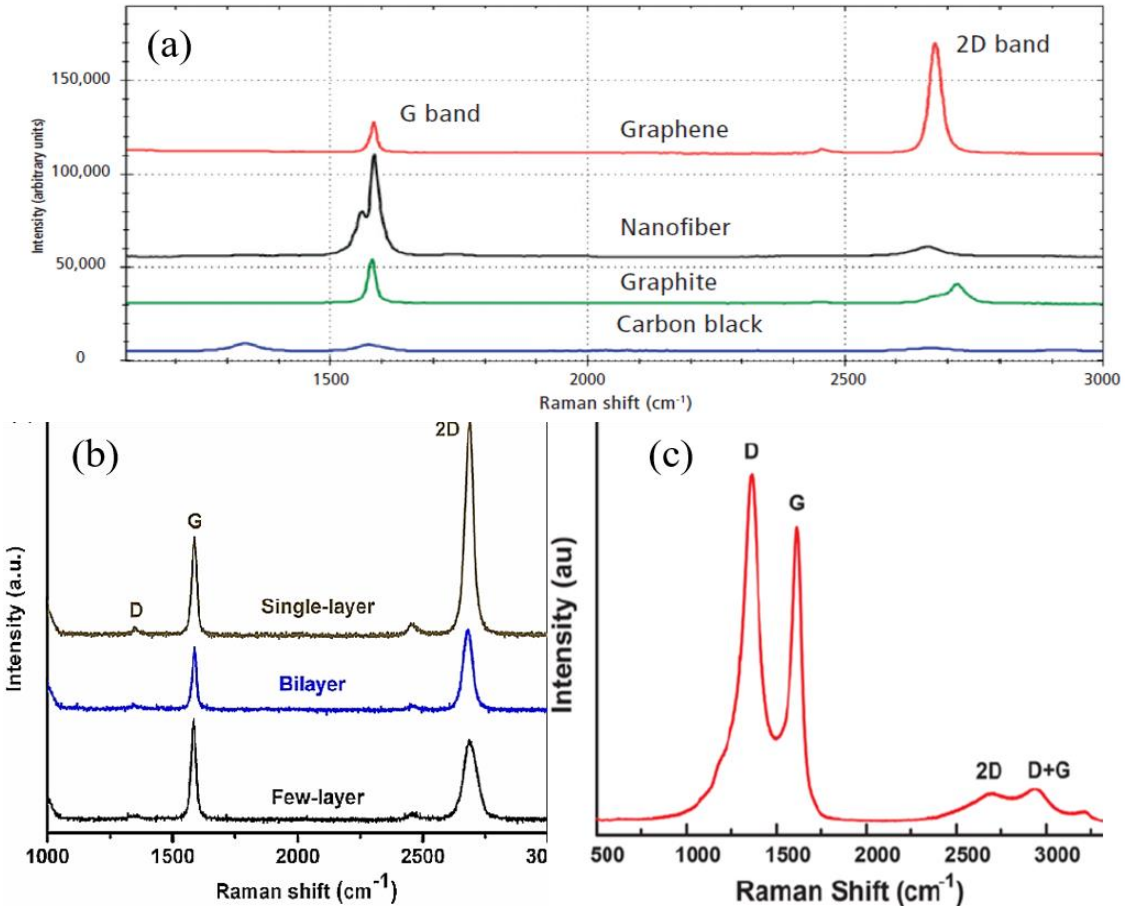

Figure 25. Reference Raman spectrum of carbon allotropes. (a) Typical Raman shift of carbon allotropes. (b) Raman shift of single layer graphene and stacked graphene. (c) A mixture [39]

D-peak and G-peak in Raman spectra are the most representative signal of Carbon material. D-peaks appearing at 1350 cm^{-1} arise from the breathing mode of sp^3 hybridized carbon atoms. In addition to this, stretching between any pair of the sp^2 hybridized carbon atoms leads to G-peak at 1560 cm^{-1}. G-peak is the chemical signature of graphitic material. It exists in all types of crystalized carbon allotropes except diamond, because a C-C bond in diamond is sp^3 hybridized. The high intensity of D-peak indicates numerous C-C bonds are defective in the structure; instead of formation of a sp^2 C-C bond, a carbon

atom forms a sp^3 bond with a hydroxy group and turns into graphene oxide. Therefore, D-peak is not a desired signal for grapheme, because the higher intensity of D-peak, the lower the quality of graphene. Hence D-peak signifies the presence of graphene oxide in the sample. The ratio of D-peak intensity and G-peak intensity, I(D)/I(G), is the critical factor in evaluating the value of graphene material. Large I(D)/I(G) numbers describe either a high structural defect ratio in the graphene sheet or a low rate of reducing reaction of graphene oxide.

For Raman spectral analysis, Kapton films were carbonized using different doses of laser using the same laser engraving system: Both power and engraving speed of the writer were modified to create two distinct laser doses. A wide-range (0-10000 cm^{-1}) Raman scan was performed on both samples, but only signals between 1000-4000 cm^{-1} were extracted, because peaks of carbon allotropes fall into this range. Plots of the Raman spectrum of both samples are presented in Figure 26, which includes peaks that can be associated with allotropes such as Carbon black (amorphous carbon, a-C), graphite, graphene, and graphene oxide. The increasing laser dose raised the intensity of all peaks except carbon-black (D+G), which leads us to conclude that a more crystalized carbon was produced by a higher power and dose. 2-D peak also increased after high laser dose, and the higher intensity of the peak means that there is an increasing concentration of graphene content in the conductive LSC layer. The ratio between the intensity of G-peak and 2D-peak demonstrates the stacked nature of the multiple layers of graphene; a larger I(G)/I(2D) indicates more layers of graphene stack in the system. According to the results in Figure 24, this ratio dropped slightly from 1.12 (278/248) to 1.08 (312/288). Hence an increasing laser dose led to an increase in graphene found in the LSC layer. A wider D-

peak and G-peaks with additional shoulders indicate that the crystal structures and size of graphene oxide and graphite may also be affected as laser power is increased. Furthermore, more measurement noise occurred in the high-power sample, which may come from the resin particles produced during the high power exposure. Further study may be necessary to determine the cause of increasing noise.

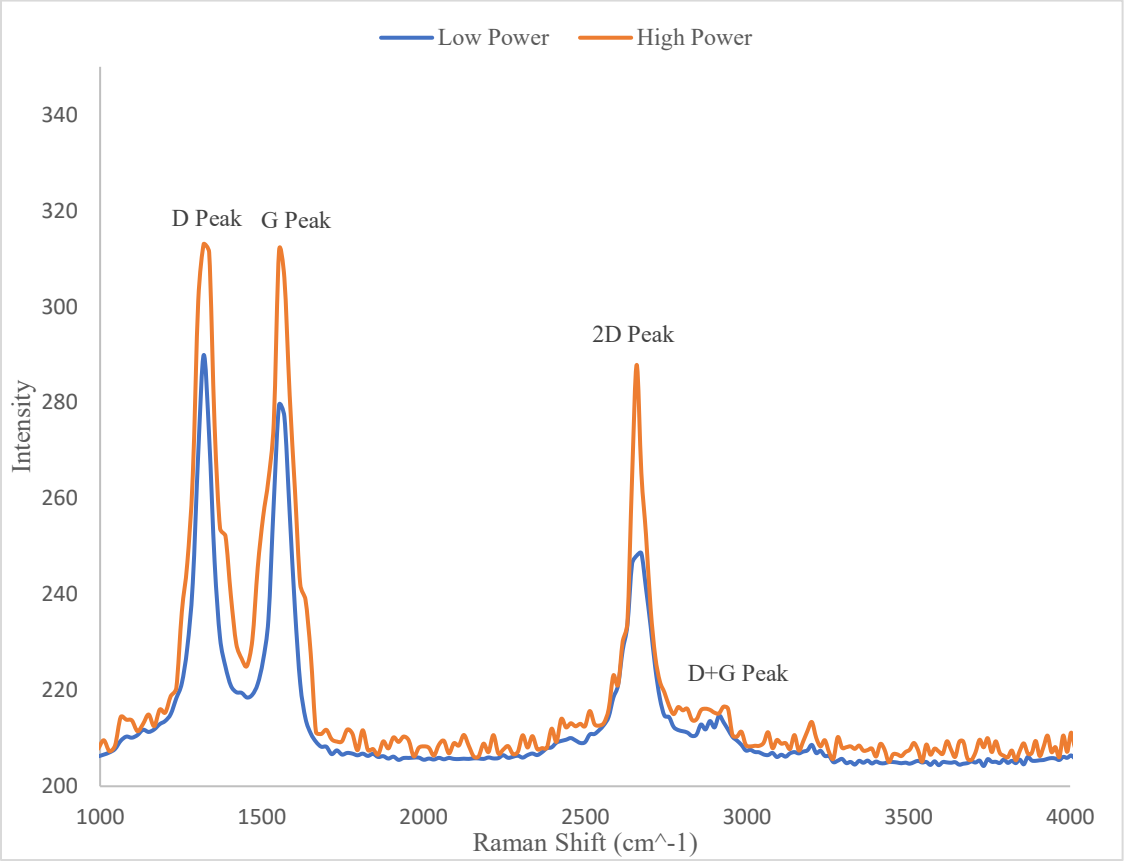

Figure 26. Raman spectrum of carbonized Kapton fabricated using different laser dose

Varying the laser power and dose to carbonize cardboard also causes a significant change in the ratio of carbon allotropes. According to the result in Figure 27, the amount of graphene is negligible in the resulting LSC layers fabricated with a low laser dose. However, considerably more graphene could be observed when a larger laser dose was

used to carbonize the surface of cardboard. Additional shoulders at the base of the D+G peak of LSC on cardboard are wider than the D+G peak of LSC on Kapton (Fig 26), which indicates that LSC on paper contains more graphite than LSC on Kapton. Also, the substantial increase of D-peak shows that more graphene oxide results from paper as compared to Kapton. Hence, paper might provide a low-cost opportunity to produce graphene oxide rich carbon layers that may be beneficial for certain sensor applications

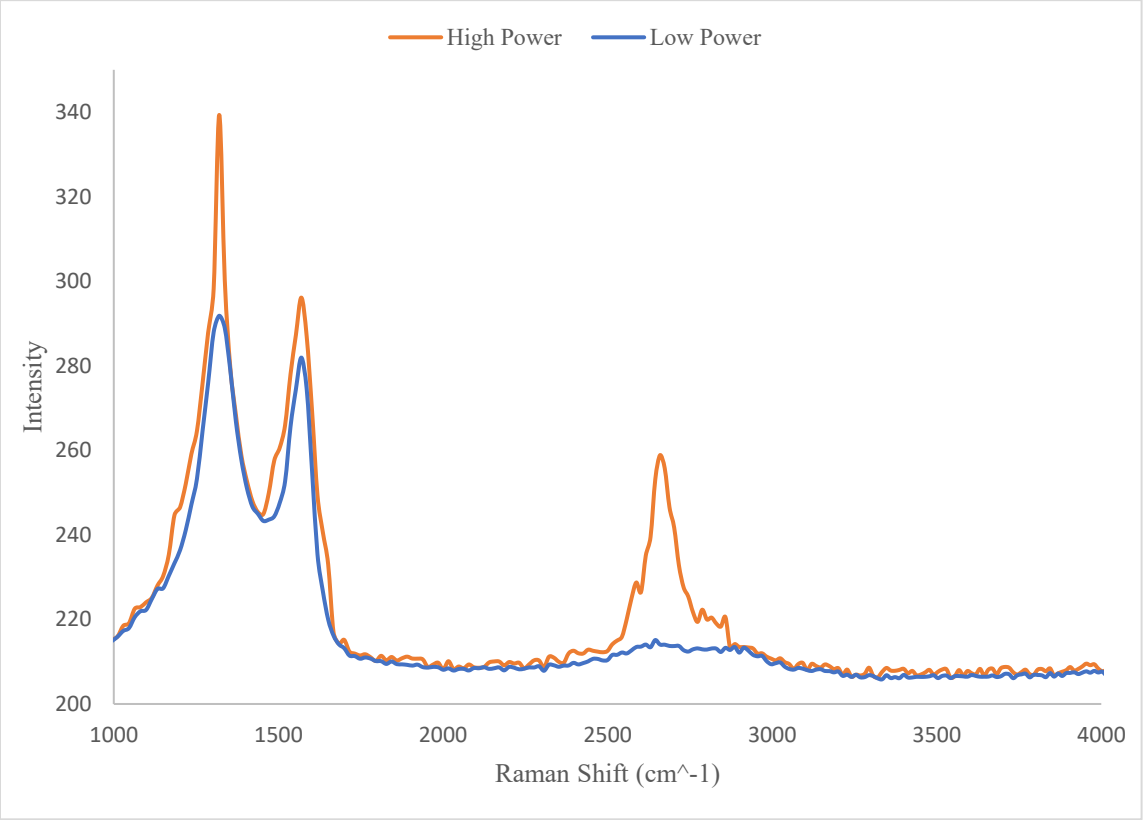

Figure 27. Raman spectrum of carbonized cardboard fabricated using different laser dose

In order to study the spectral properties, the LSC layer of wood was initially transferred to adhesive tape once fabrication was finished. The result in Figure 28 indicated a markedly different spectrum that is indicative of a composite LSC layer on wood material. Although researchers from Rice University [15] carbonized wood to

produce functional graphene-based devices, their laser system used a mid-IR (λ~10μm) CO_2 laser that also has substantially higher power (40W) than the available system in our lab.

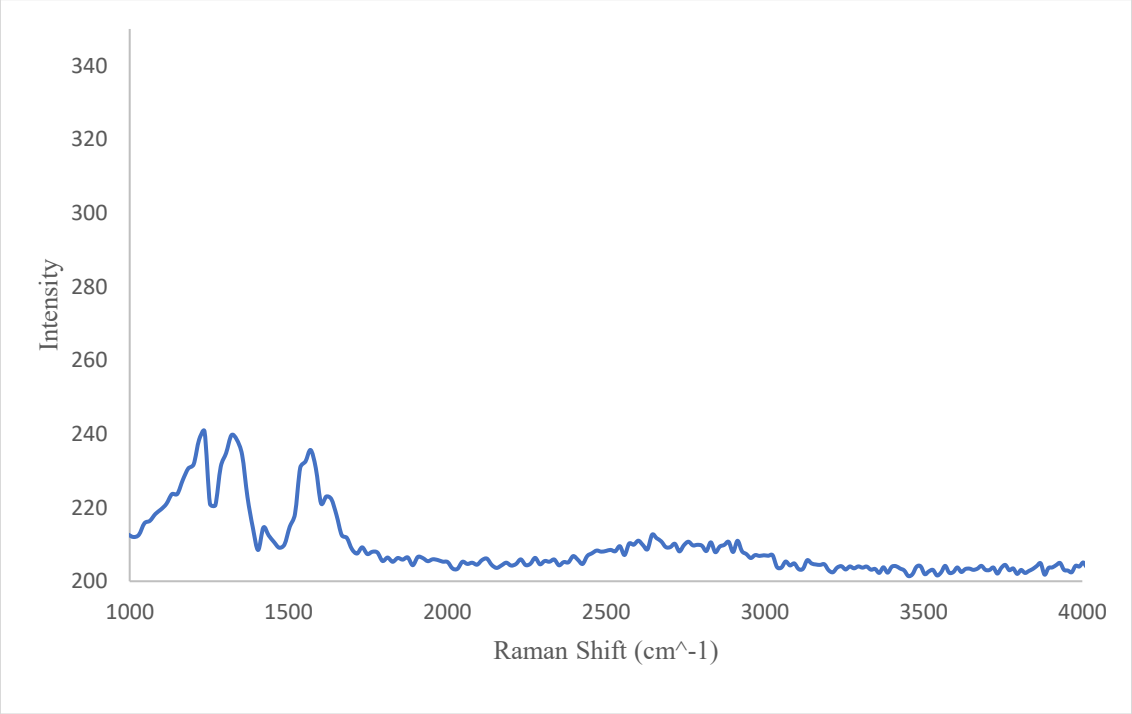

Figure 28. Raman spectrum of carbonized wood

3.6 Aging and Degradation

High quality Carbon structures with fully formed bonds and their allotropes are typically not chemically activated. However, the structures with large numbers of defects and dangling C-bonds change this picture. Consequently, complex porous structures found in our LSC layer should be capable of absorbing a large amount of various chemical compounds, i.e. ideal for sensing applications. However, this also implies that the LSC layers may be vulnerable to aging and exposure to uncontrolled atmospheric conditions. When the absorption occurs on the LSC layer on a substrate, it is believed

that those chemicals significantly influence the electrical properties of the LSC layer. To study this issue, we also implemented an aging study; a laser fabricated device was attached to measuring probes, and the setup would be held free from any physical motion or environmental extremes such as excess temperature or humidity during the experimental period to ensure the consistency of probe-LSC contact surface.

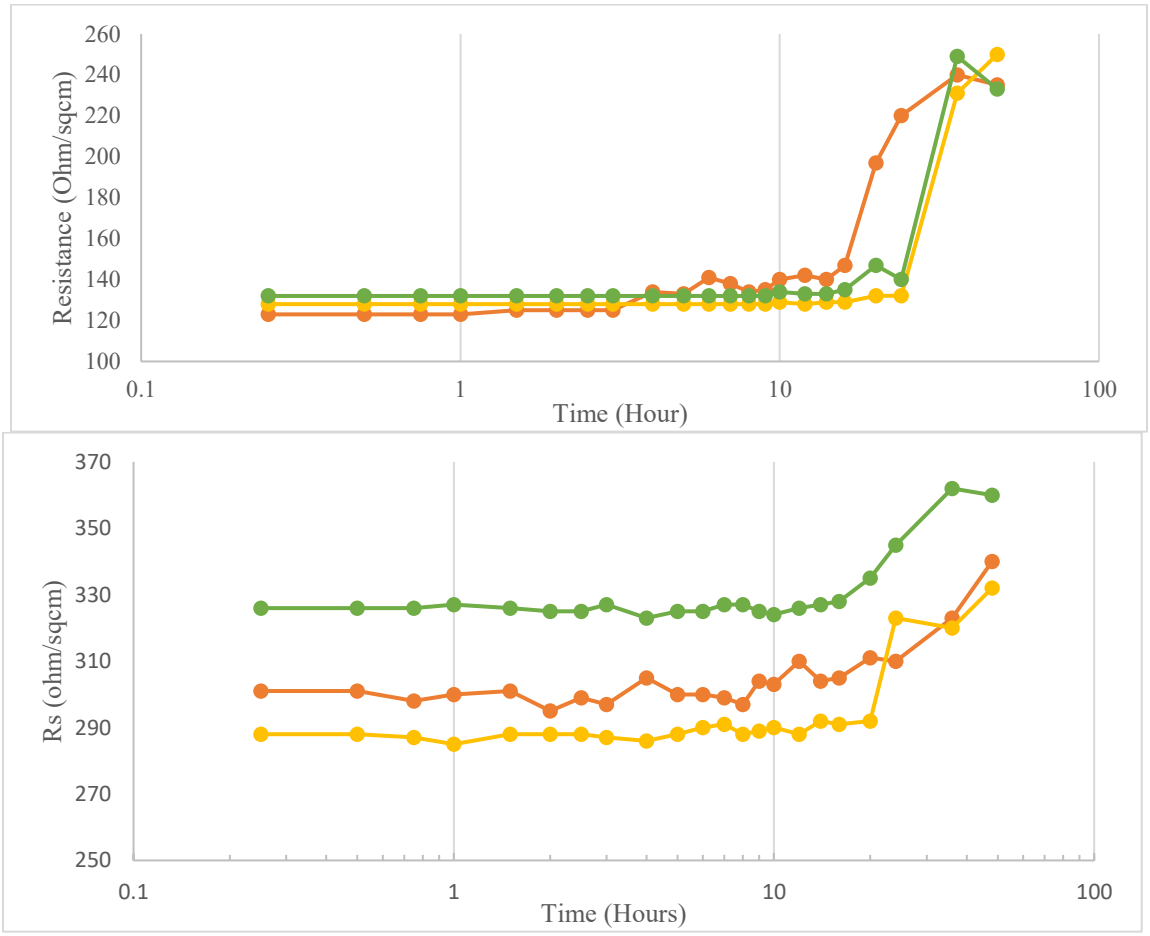

Figure 29. Resistance changing of LSC on Kapton (top) and cardboard (bottom) over time

The results in Figure 29 show the resistance of LSC on Kapton and cardboard changed significantly within 48 hours. For repeatability, three samples were studied for

both Kapton and cardboard samples. The figure indicates that exposing the LSC layer on Kapton to the atmosphere results in roughly doubling the resistance at the end of 48 hours. However, the process is highly non-linear and the LSC remains fairly stable during the first 8 – 9 hours of exposure to atmosphere. One of the samples shows slightly more sensitivity to the atmosphere. More importantly, the most dramatic changes to LSC resistance occurs at the end of 24 hours when Kapton resistance starts rising in a sharp fashion in the next 24 hours before saturation. A more sensitive sample undergoes these changes markedly earlier. Although a similar pattern is observed for the cardboard samples, the overall change of LSC resistance is less dramatic and the rise is more gradual. Cardboard samples start oxidizing after ~10hrs and their resistance goes up by a mere ~15%, In either case, the optical and scanning electron microscope imaging did not reveal a distinguishable change of LSC morphology on both substrates after exposure to the atmosphere. Thus, this unique analysis shows that for more reliable and repeatable results, the LSC layers should either be encapsulated or stabilized in device/sensing applications.

CHAPTER 4: PROTOTYPE OF LASER ENGRAVED DEVICES

Chapter 3 examined the optimal operation parameters for producing the least resistant LSC on Kapton and cardboard materials, which will be used in the present chapter to form practical devices. However, before starting such an effort it is very useful to understand if the proposed process (speed=1100mm/min, power=60unit and density=16line/mm) shows high repeatability. Table 5 lists sheet resistance measurements of five resistors fabricated using the same optimal laser dose on Kapton and cardboard; a cooling period of at least thirty minutes was provided for the laser system between each fabrication to ensure the intensity and efficiency of the laser head, and the quality of the conductive layer is high.

Table 5: Measurement of linear resistor fabricated using optimal parameters on Kapton and cardboard

Trail Number	Resistance (Ω/cm)	
	Kapton	Cardboard
1	114	215
2	123	222
3	110	218
4	103	237
5	129	239
Average	115.8	226.2
Standard Deviation	8.9%	4.9%

However, in a bar bell shape resistor, it is observed that resistance increase is non-linear with the length of the resistor. Hence another factor is thought to play a part. Isolated single lines scribed using the same process (see Figure 30), indicate that the

width of line is not uniform, which is responsible for this non-linear variation and is caused by the unstable power output of the laser head. The heat sink of the laser head is not designed well, therefore, extended continuous illumination of laser head would lead to heat variations and an unstable light output which is similar to a sine wave, because the thermal coefficient of the diode is negative and as such causes sizeable negative feedback. We cannot exclude the mechanical vibration caused by the mechanical belt-drive system either. Although unfortunate this is not surprising, as the sub-par performance is a consequence of working with an ultra-low cost (hobby-level) engraver. We expect such errors to diminish once we acquire a professional-level system with higher quality optics (beam size ~10 microns), stepper accuracy of ~1micron, and proper thermal and mechanical stability of the laser driver.

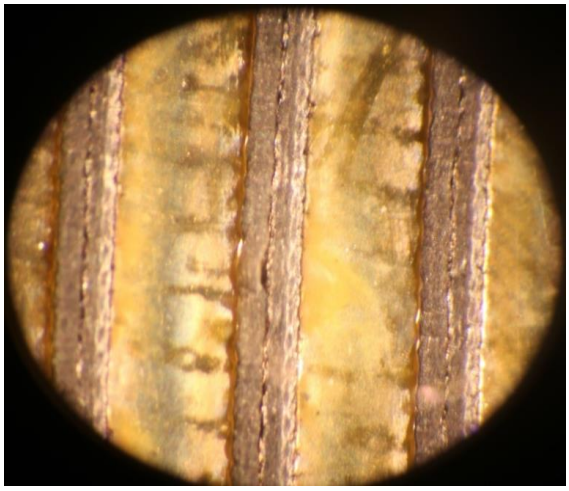

Figure 30. Single line scribing of laser on Kapton film

4.1 Capacitor

Interdigitated electrodes (IDE) are extremely important components in printed electronics. Besides working as planar capacitors, they are also an effective configuration

for many resistive sensors which have high sensitivity and low contact losses. A conventional planar capacitor has limited flexibility and can easily deteriorate in performance if the dielectric layer has DC leakage or high AC losses. IDEs formed by conductive LSC electrodes formed on Kapton provide a simple one-step fabrication method with no solution-based processing.

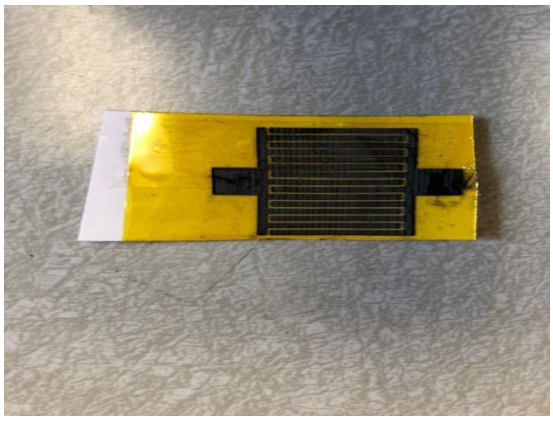

Figure 31. A laser fabricated capacitor on Kapton film which has 15 fingers

4.1.1 Electrode Spacing and Capacitance

Figure 31 shows a laser fabricated capacitor on Kapton: two sets of electrodes in capacitors have a total of 15 fingers separated by a distance of 0.5 mm. The performance of the capacitors was tested using Agilent E4980A LCR meter at a frequency of 100 kHz. The measured capacitance on Kapton is 3.11 pF, while the same design on the cardboard forms a capacitor of 1.76 pF, with phase angles of 88.56° and 86.12°, respectively. Given that two capacitors have ideally the same dimensions, the dielectric constant (ε_r) of Kapton® and paper is ~4.5 and ~2.5, respectively, and the top side is air (ε_r=1); the capacitive difference should be (4.5+1)/(2.5+1)=1.57. The measured ratio of

3.11/1.76=1.77 is 13% greater than the theory predicts, which is close enough given the ~9% and ~5% standard deviations on each substrate material given in Table 5.

Table 6: Measurement of 15-finger capacitors have 0.5 mm electrode space, 15 mm finger length

Trail Number	Kapton		Cardboard	
	Capacitance (pF)	Phase Angle (Deg)	Capacitance (pF)	Phase Angle (Deg)
1	3.11	-88.56	1.76	-86.12
2	2.74	-89.33	1.85	-87.34
3	3.93	-88.17	1.83	-87.91
4	3.48	-88.62	1.74	-87.87
5	3.62	-88.44	1.83	-86.30
Mean ± Std. Dev.	3.38±19.4%	88.62±0.4%	1.80±6.1%	87.11±1.0%

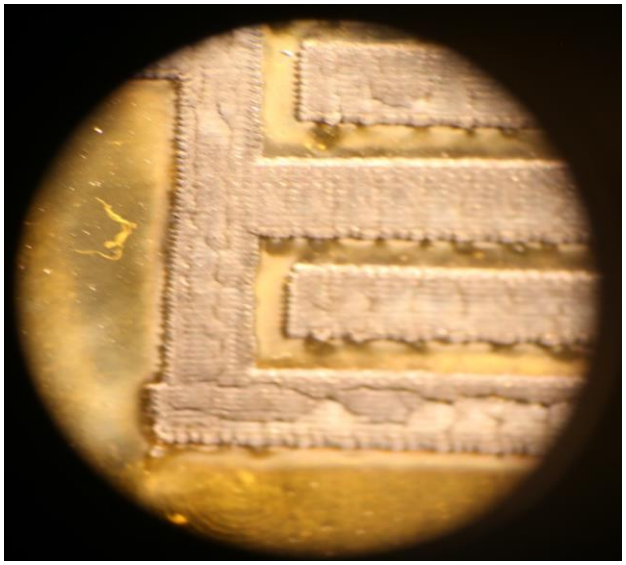

Figure 32. Non-uniform distance between capacitor electrodes on carbonized Kapton

Table 6 and Figure 32 lend additional support for the significance of process variations. The statistical data obtained from five Kapton capacitances vary in a relatively large range (±19.4%), and a capacitor on cardboard has a smaller standard deviation (±6.1%). The microscope images in Figure 32 illustrate that the edge of the capacitor electrodes can be rather rough. The distance between carbonized electrodes on Kapton film is not uniform because LSC growth is not necessarily in a single direction. This causes variations in electrode spacing, and capacitance would be also varied as a result. Table 6 also shows that cardboard devices have more uniformed electrode spacing and more consistent results. LSC growth on cardboard is different from LSC growth on Kapton. Unlike carbonized Kapton that has a significantly higher overall thickness, Dek-Tak measurements indicate that carbonization leads to minute changes of overall thickness on cardboard. LSC on cardboard grows toward to the inside of cardboard; the higher the laser dose, the deeper the LSC becomes. In other words, a lack of outgrowth in LSC electrodes is the main cause of the clear interface and more stable capacitor on cardboard.

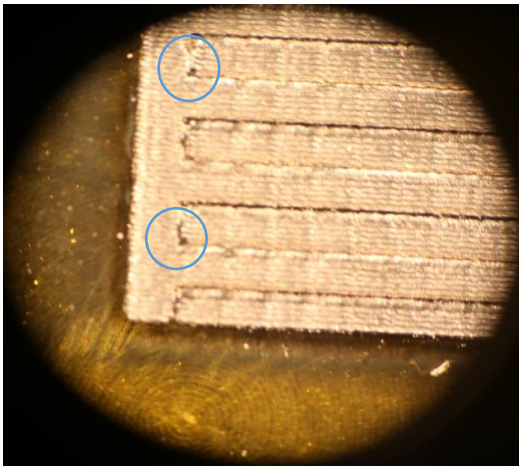

Figure 33. Electrodes may short out due to rapid growth of LSC layer in high doses.

Although the specified minimum resolution of the laser engraver system is ~0.1mm, experimental results show that overlapping of electrodes frequently occurs when spacing is smaller than 0.5mm. Therefore, a moderate laser dose that slows down the outgrowth of LSC layer is desirable to fabricate devices with electrode spacing less than 1 mm. Indeed, the picture in Figure 33 shows shorted electrodes caused by excessive growth of LSC lines on Kapton at very large doses. Increasing electrode space from 0.5 mm to 1.5 mm decreased capacitance of the 15-finger capacitor on Kapton from 3.58 pF to 2.17 pF and phase angle varies in a range of ± 3.6%, which is not significantly affected by larger electrode spacing.

Table 7: Relationship between electrode space and capacitance

Electrode Space (mm)	Kapton		Cardboard	
	Capacitance (pF)	Phase Angle (Deg)	Capacitance (pF)	Phase Angle (Deg)
0.5	3.58	-88.54	1.89	-87.24
0.6	3.35	-88.67	1.63	-87.75
0.8	3.24	-85.13	1.55	-80.13
1.0	2.81	-83.26	1.41	-82.93
1.2	2.72	-81.84	1.33	-83.76
1.5	2.17	-82.21	1.22	-83.17

Increasing electrode space decreases capacitance on cardboard devices as well. When electrode space increased from 0.5 mm to 1.5mm, the capacitance of the cardboard

capacitor dropped from 1.89 pF to 1.22 pF; meanwhile, the phase angle remains stable just as observed with LSC devices on Kapton.

4.1.2 Electrode Dimensions

This section examined the correlation between the shape of an electrode and its capacitance. The total surface area of an electrode contributes significantly to the capacitor values when electrodes have fixed spacing. Increasing the surface area of electrodes results in larger capacitances. The surface area of an electrode is determined by the length and number of fingers on each electrode when the device is single layered. Table 8 summarizes the observed capacitance trends for different electrode lengths.

Table 8: Relationship between length of finger and capacitance

Length of Finger (mm)	Kapton		Cardboard	
	Capacitance (pF)	Phase Angle (Deg)	Capacitance (pF)	Phase Angle (Deg)
5	2.92	-87.84	1.79	-88.42
7	3.21	-87.22	1.76	-87.39
10	3.36	-88.94	1.84	-86.82
15	3.52	-82.77	1.94	-80.96
20	3.67	-78.90	2.21	-69.44
30	3.94	-61.42	2.98	-55.29

Figure 34 demonstrates capacitors that have 5 mm fingers and 10 mm fingers, respectively; each electrode has 15 fingers, and the space between fingers was set to 1 mm. Measurement results support that increasing the length of fingers has a positive

correlation to capacitance; increasing finger length from 5 mm to 30 mm results in approximately a 30% increase of capacitance. This is because highly elongated electrodes lead to a significant increase in series resistance and the associated decrease of phase angle. LCR meter measurement indicates that LSC capacitors on Kapton and cardboard which have 30mm fingers have an average phase angle of -61.42±12.44% and -55.29±23.76% respectively. A phase angle lower than ~85° is not acceptable, as it is indicative of high series resistance, which is believed to be caused by relatively high sheet resistance of elongated LSC layers. Section 3.4 already discussed that scribing long lines creates numerous defects and uniformity concerns in LSC layers due to poor heat control caused by the laser diode. Lowering the power level of the laser reduces the loss of phase angle, although multiple engraver passes will be necessary. Indeed, if a power level of 0.5 W is used to fabricate the same 30-finger capacitor on Kapton, the phase angle partially recovers to 79.43±15.71%.

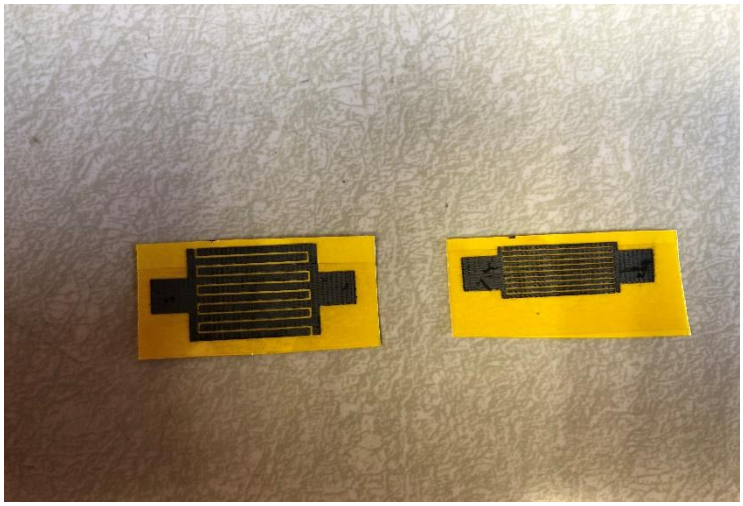

Figure 34. Capacitors have various finger size of 1mm (left) and 0.5 mm (right)

Capacitors which had a 10 mm length finger and 0.5 mm electrode space were used to study the effect of the number of fingers on IDE capacitance. Results in Table 9 indicate that an increasing number of fingers raises the surface area of the capacitor electrodes, and by default also the measured capacitance. When the number of fingers was increased from 10 to 30, the capacitance on Kapton devices increased from 2.38±13.71% to 6.49 ±18.21%, and capacitance on cardboard increased from 1.43±10.45% to 2.91±14.61%. The phase angle showed a slight decrease on both Kapton and cardboard; this phenomenon is caused by the reduced efficiency of laser heads in all likelihood because of a slight overheating of the laser diode in the extended writing session.

Fabricating large devices seems challenging. Defects in the LSC layer and overheating of the laser system limit the quality and yield of devices. A series of experiments proves that utilizing low power to carbonize a substrate multiple times significantly improves the quality of a large area LSC layer; however, high-accuracy positioning of the laser system is critical because the mismatch of each layer may cause the whole device to be non-functional. As a result, the existing laser system must be upgraded to ensure reliability in producing large area LSC devices.

Table 9: Relationship between number of finger and capacitance

Number of Finger	Kapton		Cardboard	
	Capacitance (pF)	Phase Angle (Deg)	Capacitance (pF)	Phase Angle (Deg)
10	2.38	-88.87	1.43	-88.73
15	3.43	-88.94	1.78	-87.91
20	5.01	-88.12	2.24	-88.40
25	5.97	-88.85	2.91	-87.84
30	6.49	-87.99	3.38	-87.67

4.1.3 Lifetime Test of Capacitor

The previous chapter discussed that conductivity of a porous LSC layer can be compromised in the atmosphere due to the absorption of humidity and oxygen. Resistance of LSC layer on Kapton and cardboard increases dramatically over 48 hours, and may lose conductivity permanently after an extended atmospheric exposure. Such degradation could happen as well on the capacitor due to increasing losses and a poor phase angle. To verify the assumption, a capacitor was transferred to the LCR measuring setup once fabrication was finished and the contact between capacitor and probes remained steady for 48 hours until the experiment was finished.

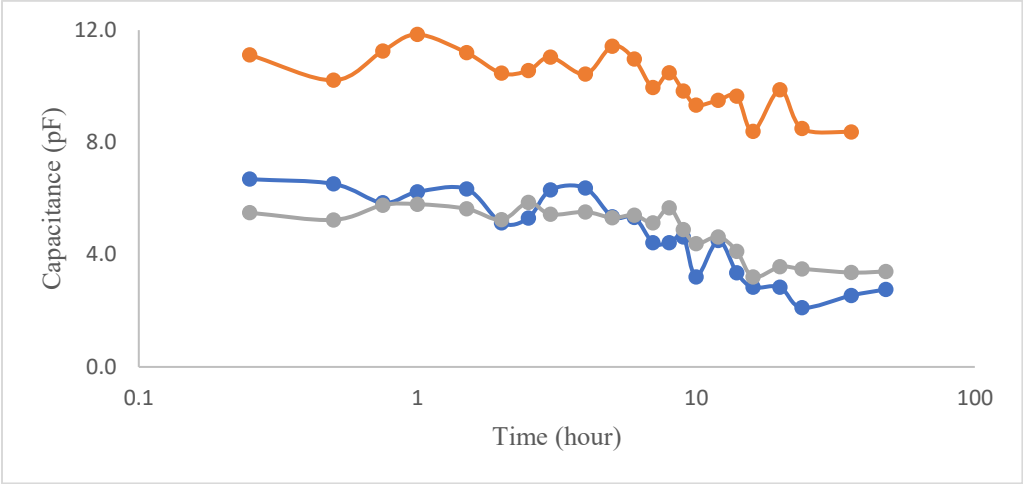

Figure 35. Lifetime of laser fabricated capacitor on Kapton

Figure 35 shows the change of capacitance of devices on Kapton film in 48 hours, with the time axis modified to a logarithmic scale to adapt a long measuring range. After 48 hours exposure to the atmosphere, the capacitance of LSC capacitor dropped, on average, by 44.38%. The decrease of capacitance was more significant after the initial ~5 hours' exposure. Additionally, the phase angle of capacitor dropped from ~88.27 to ~54.56 at the 12th hour, largely remaining the same afterward. The large decrease in capacitance and poor angle leads to the notion that capacitors are not viable after first 5 to 10 hours.

The capacitance of cardboard devices is also quite sensitive to the atmosphere. After 10 hours' exposure to atmosphere, the LSC capacitor on cardboard became totally non-functional. The phase angle of LSC capacitor dropped also in a catastrophic manner from ~87.81 to~30.74 in 10 hours. It is believed that absorbed moisture causes short circuits in a cardboard substrate because cellulose-based material has an extremely high water absorbency. Although Kapton also absorbs moisture from the atmosphere, the absorption saturates at an upper limit of 2.1% material weight. Kapton remains insulating

after absorbing this level of moisture. Porous cardboard and other cellulose-based material, on the other hand, can absorb water twice as much as their material weight, and the ionic flow percolating via the pores of LSC layer turns the insulating material into conductive material.

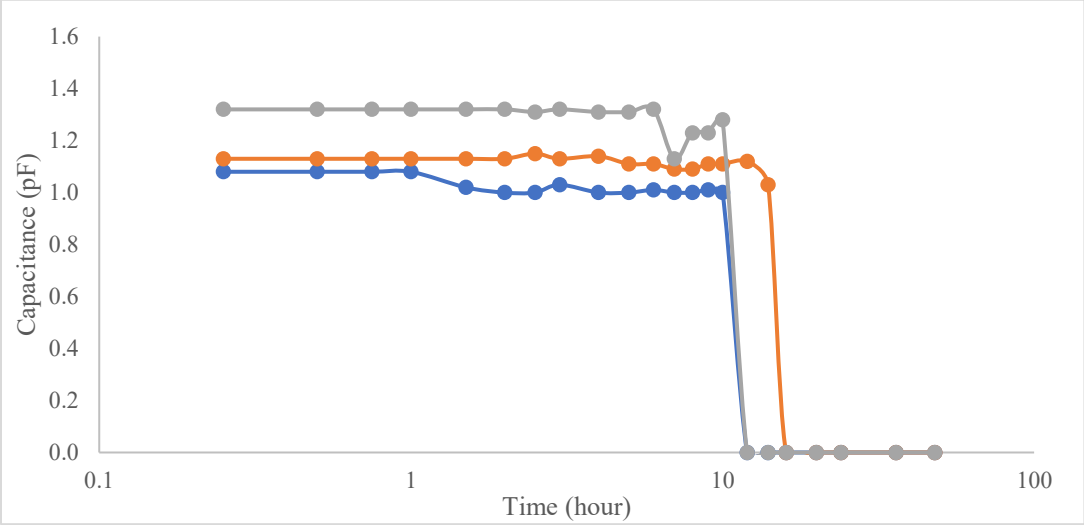

Figure 36. Lifetime of laser fabricated capacitor on Kapton

4.2 Bending Sensor

Figure 37 shows an optical picture of a bending sensor fabricated with the same laser engraver on Kapton film. This configuration of sensor is expected to change its resistance when the substrate bends in different directions. The line width of the sensor was designed to be 0.5 mm, with a functional line length of 30 mm and electrode spacing of 1 mm. Moreover, the resistance between two connection pads has an average value of 4.59±9.13% kΩ.

Cardboard is not a desired substrate for this particular application because of its brittleness. Cardboard is a cellulose-based material which has relatively short fibers,

therefore, a permanent fracture occurs once sufficient force is applied. However, bending a sensor on cardboard could be a low-cost, single-use bending sensor which acts like a "force-sensitive fuse"; when deformation happens, the cardboard substrate and conductive LSC layer break together and disconnect the circuits.

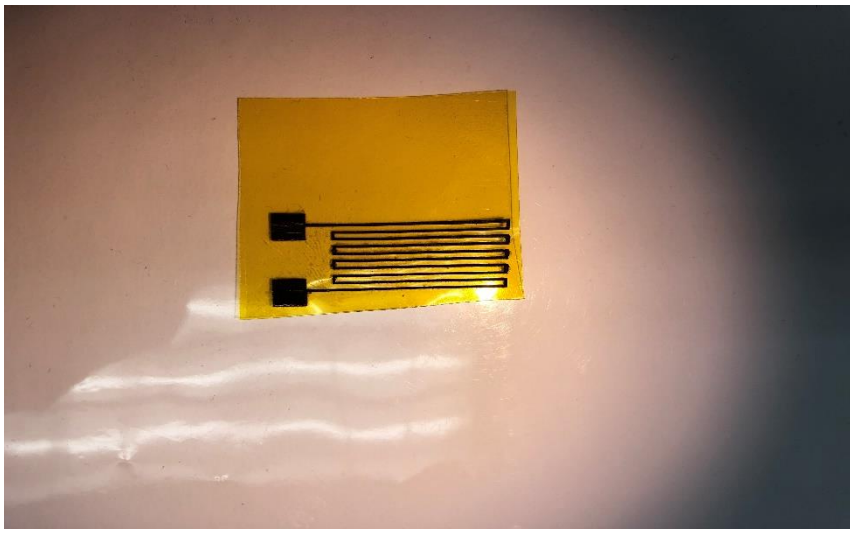

Figure 37. Optical image of bending sensor

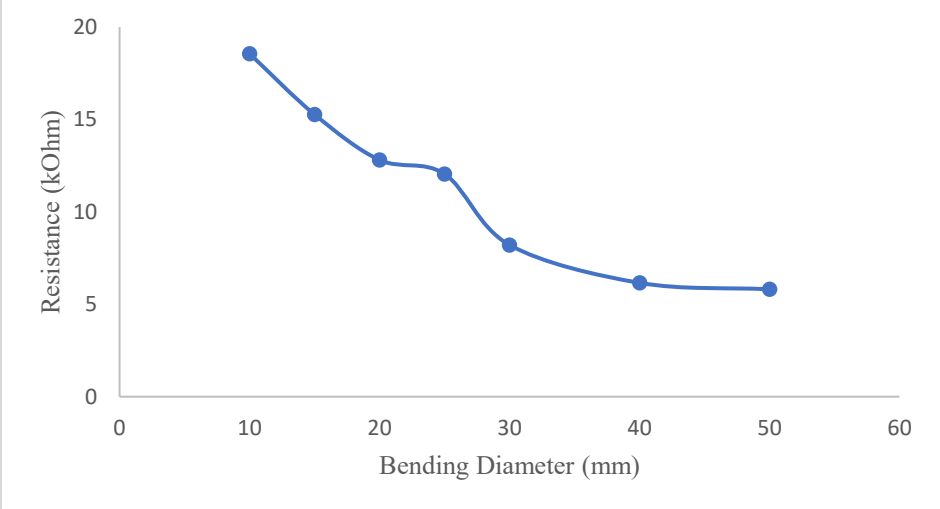

Figure 38. Resistance change over outward bending

When the Kapton sensor was bent in outward, substrate to substrate direction, the high bending curvature applied to the sensor resulted in increasing resistance, as can be seen in Figure 38. When bending diameter decreased from 50 mm to 10 mm, which means more bending was applied to the sensor, the measured 2-terminal resistance increased by 387% ± 12.36%. Such a dramatic rise in the resistance of sensors is caused by physical damage in the LSC layer, as evidenced by the optical microscope image in Figure 39 that shows the cracked surface of the LSC layer. The resistance recovers mostly if the bending movement is moderate (>40mm) because of the limited elasticity of the LSC layer, but extreme bending causes permanent damage to the sensor resistor due to the large cracked gap.

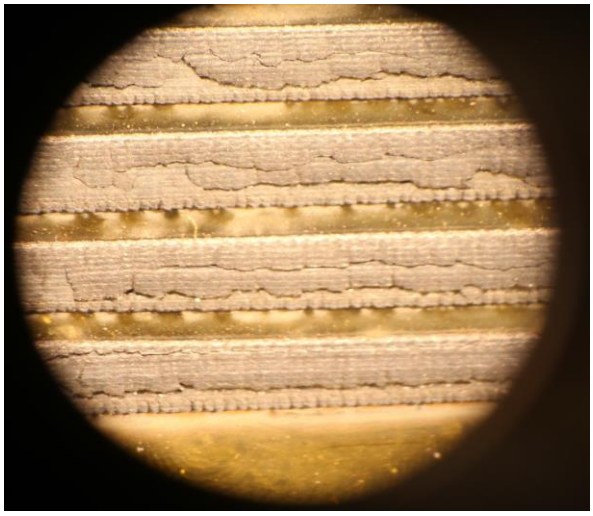

Figure 39. Damaged electrode of bending sensor

Inward bending was expected to reduce the resistance by squeezing the LSG layer. Unlike outward bending, inward bending seems to have a mild influence on the resistance of a LSC layer. Experiment results presented in Figure 40 show that when reducing the bending diameter from 50 mm to 10 mm, only ~47.17% reduction in

resistance was measured from multiple trails. The resistance of the sensor typically goes back to the approximate original value when the substrate rebounds to a flat shape.

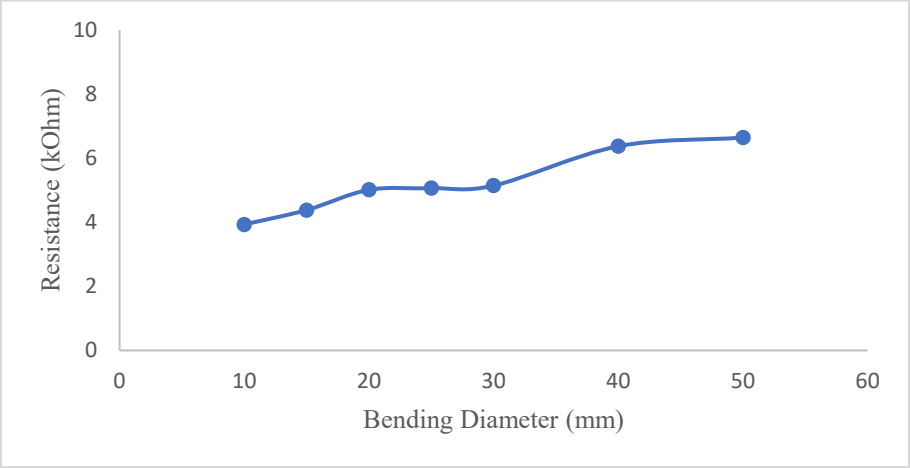

Figure 40. Resistance change over inward bending

Another unique observation was the marked delay in the response of the bending sensor burnt on Kapton film via the laser carbonization method. A change in resistance could not be observed as soon as the bending movement finished, because the reading of resistance takes a while to become steady, up to 15 seconds. Moreover, this type of bending sensor shows less sensitivity to minor movement. The series of bending experiments shows that a bending movement which has a diameter below 5 mm cannot lead a reliable change of resistance, and that a small bending movement could lead to a false result. Both the delay and low initial sensitivity are indicative of the initial elastic properties of the LSC film on Kapton, which eventually respond to large changes in resistance once sufficient damage accumulates in the network.

4.3 Three-Electrode Analytical Strip

Cyclic voltammetry (CV) is a critical electrochemical analysis method due to its high efficiency and high accuracy. Three electrodes are needed in a CV analytical cell: a working electrode, a counter electrode, and a reference electrode. A laser-fabricated device is designed as shown in Figure 41; unlike conventional CV devices, all three electrodes of laser-fabricated device are carbon allotropes formed by a carbonization reaction of the substrate.

In order to study the performance of the laser-fabricated devices, a conventional (commercial) three-electrode reference device was compared to the LSC devices burnt on Kapton and cardboard. Ivium CompactStat was used to conduct the scans and process experimental data. The electrolyte was a 0.1 M KCl solution, and the analyte was 15 mM potassium ferricyanide. Additionally, the scanning range was set to -1 Volt to 1 Volt, and the scanning rate was set to 50mV/s. Since the reaction from potassium ferricyanide to potassium ferrocyanide is reversible, a pair of center-symmetrical wave was expected from experiments, as shown in Figure 42. The CV result in Figure 42 was obtained by using an integrated commercial test strip, which has a gold working electrode, a gold counter electrode, and an Ag/AgCl reference electrode. Two peaks around 0.02 V and 0.3V respectively could be observed from the result, and the voltage values for these peaks appear to match the reference results published in the literature [12]

Figure 41. Design of three electrode system

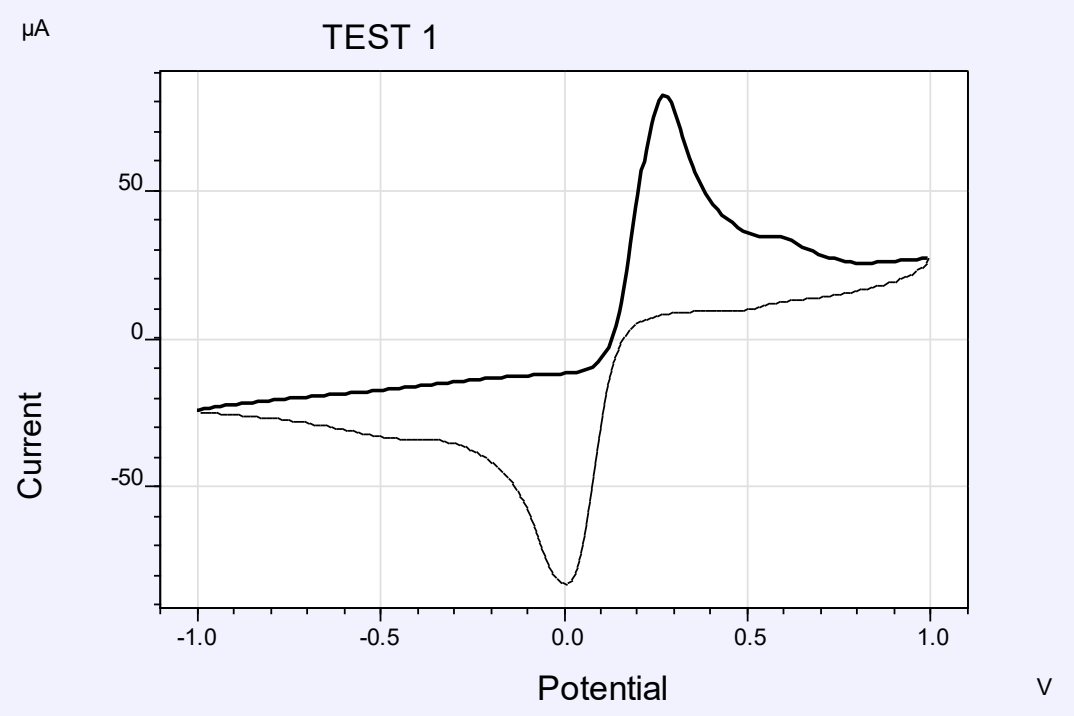

Figure 42. Cyclic voltammetry of conventional electrochemical cell which has Au, Ag/AgCl

The CV Curve in Figure 43 is the test result of 15 mM potassium ferricyanide obtained using the LSC test strip burnt on Kapton. Three continuous runs were performed in the experiment; a slight peak shift from subsequent trials occurred due to the absorption of the porous LSC layer. Unlike commercial carbon electrode, which has a glossy surface, the LSC has a very porous structure, as demonstrated in Section 3.3. This porous structure may trap a large number of ions along the reaction process, and local ion concentration on LSC electrode surface is larger than the whole system. Hence, LSC test strip seems to be more appropriate for single-use devices. Carbon layers start to loosen and exfoliate after multiple extended scans. However, the lifetime studies were

inconclusive at this time, since some strips are capable of lasting up to four scans, and some strips became nonfunctional at the second scan.

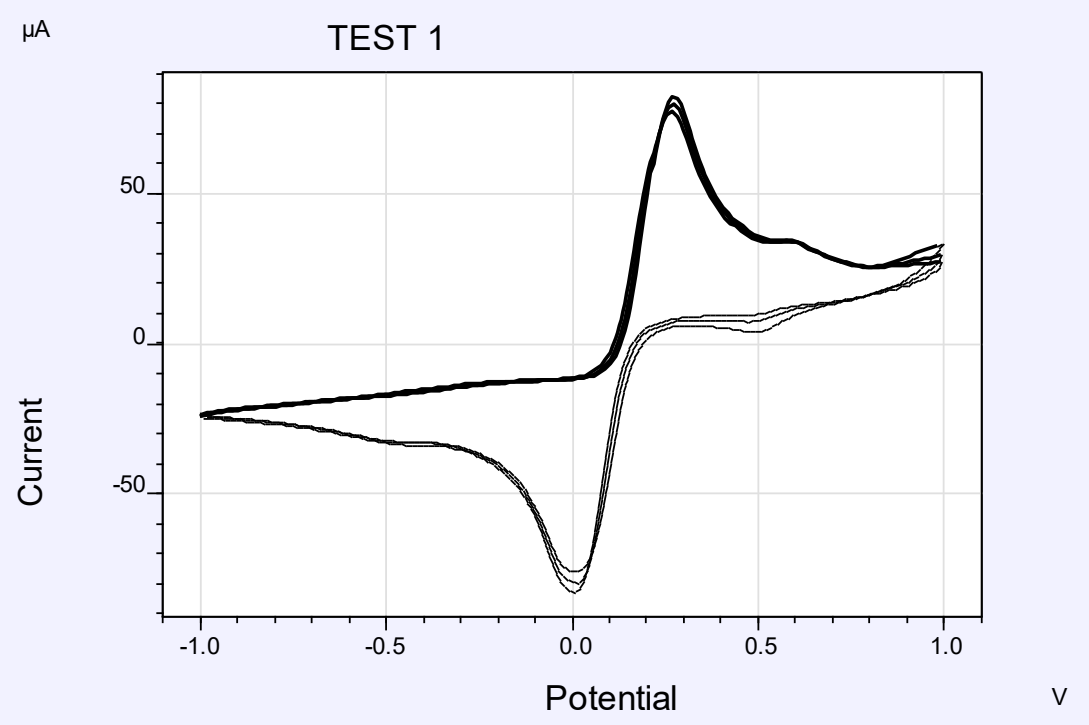

Figure 43. Repeating cyclic voltammetry of laser fabricate device on Kapton

The LSC three-electrode devices fabricated on cardboard were unable to reproduce reference results obtained from conventional electrodes. Figure 44 shows three individual CV curves for potassium ferricyanide, generated by using LSC electrodes on cardboard. Although the three curves show center-symmetrical features reminiscent of the reference sample, the crucial peak signals appear at incorrect voltage levels. The poor results are likely caused by the extremely high absorption capacity of the cardboard substrate. The peak signal is caused by the red-ox reactions between the working electrode and the counter electrode at specific voltages. However, when electrodes are supported by a very porous and absorptive substrate, the ionic flow is much slower in the

substrate material, and this results in a dramatically high local ion concentration near electrodes. The lifetime of LSC devices on cardboard is extremely short because the connection between LSC layer and substrate is rather weak. A percolating/wicking solution subjects the LSC to large shear forces due to capillary action, reducing the lifetime to only a few sweeps. Finally, gently rinsing the whole piece of cardboard that supports LSC devices with the electrolyte solution before using the test strip helps remove loose carbon particulate matter from the surface and increases reliability because that loose carbon pollutes the analyte solution and changes the conductivity of the background solution.

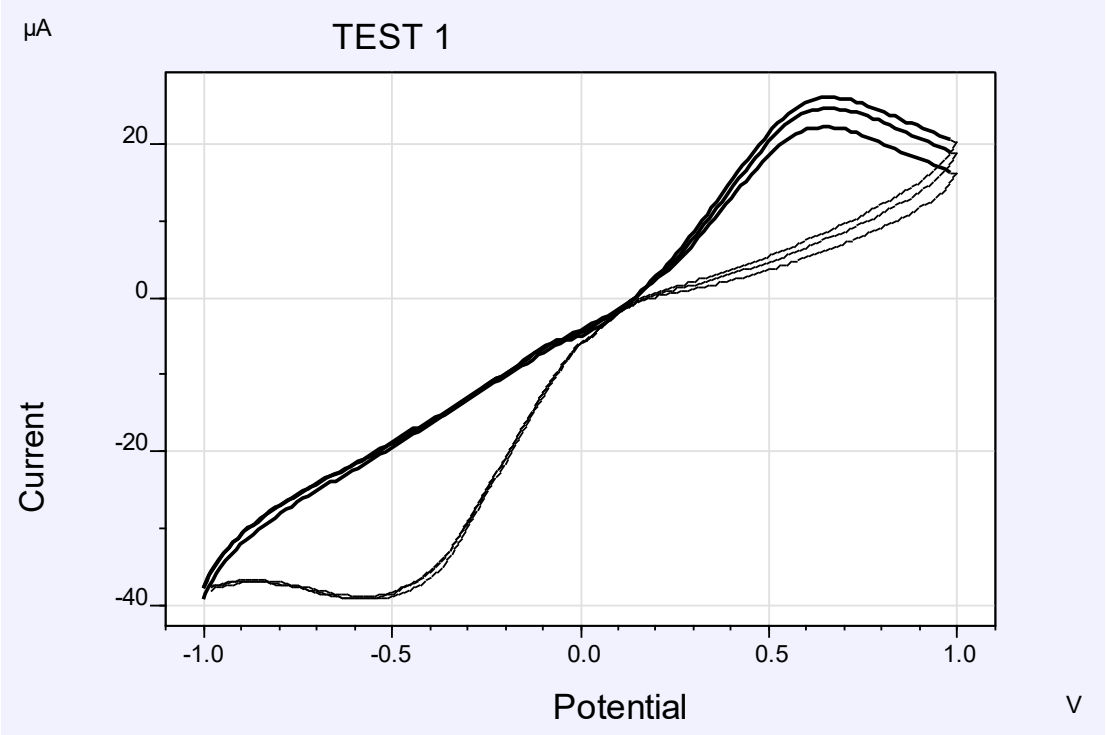

Figure 44. Repeating cyclic voltammetry of laser fabricate device on cardboard

CHAPTER 5: CONCLUSION

This study looked at the use of laser to fabricate functional electronics; the properties of a laser scribed carbon (LSC) layer on various materials were examined in a series of experiments. In addition, optimal operational parameters of laser systems were explored to enhance the electrical and physical properties of the LSC layer. Optimal writing conditions to form low-resistance layers have been determined. Tests conducted using capacitors built using this process prove that optimal process conditions and design contribute significantly to the performance of a capacitor. Moreover, bending sensor and LSC electrochemical cell experiments illustrate that LSC devices produced by a low-cost laser system function as expected.

The low-cost 2.5W laser system used in this work is capable of carbonizing Kapton, cardboard, and wood (Cedar). Publications mentioned the utilization of a CO_2 laser to fabricate a LSC layer on other polymers such as PVDF; however, experimental results show the violet laser used in this work is unable to induce carbonization on PVDF surface due to low absorption of the polymer. LSC on Kapton film fabricated with optimal parameters has an average resistance of 100 Ohm/cm^2, while LSC on chipboard paper shows an average resistance of 220 Ohm/cm^2. Resistance of LSC on Kapton and cardboard is negatively correlated to the dose of laser; however, an extremely high dose laser causes structural damage to the polymer backbone on Kapton film, and such damage leads to a significant increase in resistance. The Raman spectrum indicates that LSC fabricated with a higher dose of laser contains more crystalized carbon allotropes including graphite, graphene oxide, and graphene. Moreover, the LSC layer degrades in atmosphere over time; 48 hours' continuous measurement indicates the resistance of LSC

layer on Kapton, and cardboard remains unchanged in the first few hours, but then LSC resistance starts to dramatically increase. LSC becomes non-conductive after five days' exposure to the atmosphere. These results indicate that a protective or filler layer is required for functioning devices with an appreciable shelf/operation life.

Functional devices were also fabricated and tested in this thesis. Proper geometric design contributes significantly to the enhancement of capacitance on Kapton and cardboard. It is shown that LSC capacitors are highly sensitive to atmosphere, which is indicative of a very large surface area and oxygen sensing capability in these layers. In fact, the LSC capacitor on Kapton reduces by 44.38%, and the LSC capacitor on cardboard becomes completely unfunctional after 10 hours. A single-use bending sensor fabricated on Kapton film was tested in this work, and the resistance of the sensor changed differently at various bending degree due to surface damage caused by bending. Three electrode strips fabricated on Kapton and cardboard are capable of performing cyclic-voltammetry analysis. Three electrode strips on Kapton perform similar to commercial noble-metal-electrode system. However, such LSC test strips are essentially for single use because the surface of LSC is not as glossy as that of commercial electrodes. Since there is a large market for low-cost disposable polymer devices, it should be possible to exploit laser-scribed devices especially for portable electro-chemical applications. Test strips on cardboard perform less than ideally, because the porous structure of cardboard absorbs much of the electrolytes, and this uneven concentration causes delays of current response. In conclusion, LSC devices on Kapton film perform better than devices on cardboard because cardboard has more uncontrollable factors such as fiber structure and inert chemicals.

5.1 Challenges

5.1.1 Controlled Atmosphere

Carbonization of a substrate is a type of pyrolysis reaction in which the surrounding atmosphere would be involved, and composition of the atmosphere significantly affects the final products. In this thesis, carbonization was performed only in an atmosphere which has abundant oxygen. Oxygen might majorly contribute to the presence of graphene oxide. Hence providing a noble gas atmosphere or vacuum environment for a laser engraving system has a high probability of increasing the quality and performance of graphene in a LSC layer. Moreover, pressure control or selective introduction of residual gasses into the reaction chamber can be used to control carbon allotropes in the final layer.

5.1.2 Encapsulating and Immobilization of Carbon Layer

Based on the results of this thesis, LSC is sensitive to atmosphere and deformation. Encapsulating devices may isolate LSC from the atmosphere, and the capsule would also reinforce the mechanical strength on LSC surface. However, verification tests performed in this work show that the deposition of polymers on the LSC layer turned the carbon layer into an insulator, presumably because liquid polymers may dissolve or the resulting capillary effects can structurally harm the carbon layer. The immobilization of LSC seems necessary because the exfoliation of the carbon layer was occasionally observed due to thermal and mechanical stress during and after the burning process, and those defects negatively influence the performance of devices. Thus, an efficient method to deposit polymers on the LSC surface would improve both performance and storage lifetime.

5.2 Future Work

Further work on this research should include use of a high-power laser which also has a high resolution to improve the quality and resolution of fabrication. The current work is limited by the simplicity of the engraver, which limits the laser power, pulse height. And wavelength. Ultra-short pulses at higher frequencies and at high-power levels are expected to produce carbon layer distinguished from those fabricated by the current system [40]. Since the laser system used in this research operates with a pulse reputation of 400 Hz and cannot alter the pulse height, at present the impact of these important writing parameters are not explored. High-power and high-frequency laser irradiation may induce more crystalized carbon on the surface by multiple pulsed irradiation at same location.

Resolution limits the size of devices; the laser beam has a beam diameter of 0.1 mm, and the step motor has a resolution of 0.5 mm. Thus, the minimum future size of devices studied in this thesis were all greater than ~0.5 mm. Devices in smaller size provide better compatibility in various fields such as sensors and microfluidic devices.

The functionalization of carbon surface could also be part of future work. Carbon and its allotropes are inert to most chemical or biological molecules, and as compared to noble metal, their crystal structure provides an anchor site for many organic molecules. Developing a more robust LSC layer which contains higher content of graphene may become a promising method to reduce the cost of field effect transistors and sensors that require graphene as the conducting medium [41]

REFERENCES

[1] M. F. El-Kady, V. Strong, S. Dubin, and R. B. Kaner, “Laser Scribing of High-Performance and Flexible Graphene-Based Electrochemical Capacitors,” *Science*, vol. 335, pp. 1326–1330, 2012.

[2] V. Strong *et al.*, “Patterning and Electronic Tuning of Laser Scribed Graphene for Flexible All-Carbon Devices,” *ACS Nano*, vol. 6, no. 2, pp. 1395–1403, 2012.

[3] A. Lay-Ekuakille, G. Griffo, R. Morello, C. De Capua, and F. Spano, “Sensing system for cystic fibrosis: Modeling the detection and characterization of sweat,” *2017 IEEE Int. Symp. Med. Meas. Appl. MeMeA 2017 - Proc.*, pp. 287–291, 2017.

[4] J. Tolar *et al.*, “3D Printed Functional and Biological Materials on Moving Freeform Surfaces,” *Adv. Mater.*, vol. 30, no. 23, pp. 1707495, 2018.

[5] J. A. Rogers, T. Someya, and Y. Huang, “Materials and mechanics for stretchable electronics,” *Science*, vol. 327, no. 5973, pp. 1603–1607, 2010.

[6] M. Ying *et al.*, “Silicon nanomembranes for fingertip electronics,” *Nanotechnology*, vol. 23, no. 34, 2012.

[7] Eveliina Juntunen, Sami Ihme, Arttu Huttunen, Jukka-Tapani Mäkinen, "R2R process for integrating LEDs on flexible substrate", *Microelectronics Packaging (NordPac) 2017 IMAPS Nordic Conference on*, pp. 12-16, 2017.

[8] A. Dyadyusha *et al.*, “Flexible Electronics: The Next Ubiquitous Platform,” *Proc. IEEE*, vol. 100, Special Centennial Issue, pp. 1486–1517, 2012.

[9] H. Hoffman., “Growth Ahead for Flexible Hybrid Electronics Industry,” 2017 FLEX-Conference, Monterey, United States, 2017.

[10] Y. Qi *et al.*, “A flexible device for ocular iontophoretic drug delivery,” *Biomicrofluidics*, vol. 10, no. 1, p. 011911, 2016.

[11] M. F. El-Kady and R. B. Kaner, “Scalable fabrication of high-power graphene micro-supercapacitors for flexible and on-chip energy storage,” *Nat. Commun.*, vol. 4, p. 1475, 2013.

[12] J. Lin *et al.*, “Laser-induced porous graphene films from commercial polymers,” *Nat. Commun.*, vol. 5, p. 5714, 2014.

[13] E. E. Ortelli, F. Geiger, T. Lippert, and A. Wokaun, “Pyrolysis of Kapton® in air: An in situ DRIFT study,” *Appl. Spectrosc.*, vol. 55, no. 4, pp. 412–419, 2001.

[14] G. Xu, N. Aydemir, P. A. Kilmartin, and J. Travas-Sejdic, “Direct laser scribed graphene/PVDF-HFP composite electrodes with improved mechanical water wear and their electrochemistry,” *Appl. Mater. Today*, vol. 8, pp. 35–43, 2017.

[15] R. Ye *et al.*, “Laser-Induced Graphene Formation on Wood,” *Adv. Mater.*, vol. 29, no. 37, pp. 1–7, 2017.

[16] D. H. Kim and J. A. Rogers, “Stretchable electronics: Materials strategies and devices,” *Adv. Mater.*, vol. 20, no. 24, pp. 4887–4892, 2008.

[17] R. R. Søndergaard, M. Hösel, N. Espinosa, M. Jørgensen, and F. C. Krebs, “Practical evaluation of organic polymer thermoelectric by large-area R2R processing on flexible substrates,” *Energy Sci. Eng.*, vol. 1, no. 2, pp. 81–88, 2013.

[18] S. Yang *et al.*, “Printable Metal-Polymer Conductors for Highly Stretchable Bio-Devices,” *iScience*, vol. 4, pp. 302–311, 2018.

[19] J. P. Collman, N. K. Devaraj, and C. E. D. Chidsey, “‘Clicking’ Functionality onto Electrode Surfaces,” *Langmuir*, vol. 20, no. 4, pp. 1051–1053, 2004.

[20] Product List, Sigma-Aldrich, Available: https://www.sigmaaldrich.com/materials-science/material-science-products.html

[21] V. Zardetto, T. M. Brown, A. Reale, and A. Di Carlo, “Substrates for flexible electronics: A practical investigation on the electrical, film flexibility, optical, temperature, and solvent resistance properties,” *J. Polym. Sci. Part B Polym. Phys.*, vol. 49, no. 9, pp. 638–648, 2011.

[22] D. H. Kim and J. A. Rogers, “Stretchable electronics: Materials strategies and devices,” *Adv. Mater.*, vol. 20, no. 24, pp. 4887–4892, 2008.

[23] X. Chen, X. Han, and Q. D. Shen, “PVDF-Based Ferroelectric Polymers in Modern Flexible Electronics,” *Adv. Electron. Mater.*, vol. 3, no. 5, 2017.

[24] G. Cummins and M. P. Y. Desmulliez, “Inkjet printing of conductive materials: a review,” *Circuit World*, vol. 38, no. 4, pp. 193–213, 2012.

[25] J. Musil, F. Kunc, H. Zeman, and H. Poláková, “Relationships between hardness, Young’s modulus and elastic recovery in hard nanocomposite coatings,” *Surf. Coatings Technol.*, vol. 154, no. 2–3, pp. 304–313, 2002.

[26] X. D. Huang, S. M. Bhangale, P. M. Moran, N. L. Yakovlev, and J. Pan, “Surface modification studies of Kapton® HN polyimide films,” *Polym. Int.*, vol. 52, no. 7, pp. 1064–1069, 2003.

[27] A. C. Lua and J. Su, “Isothermal and non-isothermal pyrolysis kinetics of Kapton® polyimide,” *Polym. Degrad. Stab.*, vol. 91, no. 1, pp. 144–153, 2006.

[28] M. Pumera, “Electrochemistry of graphene, graphene oxide and other graphenoids: Review,” *Electrochem. commun.*, vol. 36, pp. 14–18, 2013.

[29] “File: Poly-oxydiphenylene-pyromellitimide.png”, “File: Polyvinylidene_fluoride .png”[Online]. Wikimedia.

[30] L. Colombo, K. Kim, P. R. Gellert, K. S. Novoselov, V. I. Fal′ko, and M. G. Schwab, “A roadmap for graphene,” *Nature*, vol. 490, no. 7419, pp. 192–200, 2012.

[31] L. Li *et al.*, “High-Performance Pseudocapacitive Microsupercapacitors from Laser-Induced Graphene,” *Adv. Mater.*, vol. 28, no. 5, pp. 838–845, 2016.

[32] “Printed Electronics | SonoPlot, Inc.” [Online]. Available: http://www.sonoplot.com/printed-electronics. [Accessed: Feb. 27, 2016]

[33] Q. Ke and J. Wang, “Graphene-based materials for super capacitor electrodes – A review,” *J. Mater.*, vol. 2, no. 1, pp. 37–54, 2016.

[34] G. Watson, “ SCEN 103” [online]. Available: http://www.physics.udel.edu/~watson/scen103/cd-focusing.html. [Accesses: May 17, 1999]

[35] B.Cummingham, “A Multilevel Approach to Modeling Planar Discharge in CO2 Lasers,” [Online]. Available: https://www.comsol.com/article/a-multilevel-approach-to-modeling-planar-discharge-in-co2-lasers/. [Access April 24, 2017].

[36] “File: three electrode setup. png” [Online]. Wikimedia.

[37] P. Suvarnaphaet and S. Pechprasarn, “Graphene-based materials for biosensors: A review,” *Sensors (Switzerland)*, vol. 17, no. 10, 2017.

[38] R. Arul, R. N. Oosterbeek, J. Robertson, G. Xu, J. Jin, and M. C. Simpson, “The mechanism of direct laser writing of graphene features into graphene oxide films involves photoreduction and thermally assisted structural rearrangement,” *Carbon N. Y.*, vol. 99, pp. 423–431, 2016.

[39] A. C. Ferrari, “Raman spectroscopy of graphene and graphite: Disorder, electron-phonon coupling, doping and nonadiabatic effects,” *Solid State Commun.*, vol. 143, no. 1–2, pp. 47–57, 2007.

[40] M. F. El-Kady and R. B. Kaner, “Scalable fabrication of high-power graphene micro-supercapacitors for flexible and on-chip energy storage,” *Nat. Commun.*, vol. 4, p. 1475, 2013.

[41] D. Yang and C. Bock, “Laser reduced graphene for supercapacitor applications,” *J. Power Sources*, vol. 337, pp. 73–81, 2017.

APPENDIX A. WAVELENGTH MEASUREMENT OF LASER

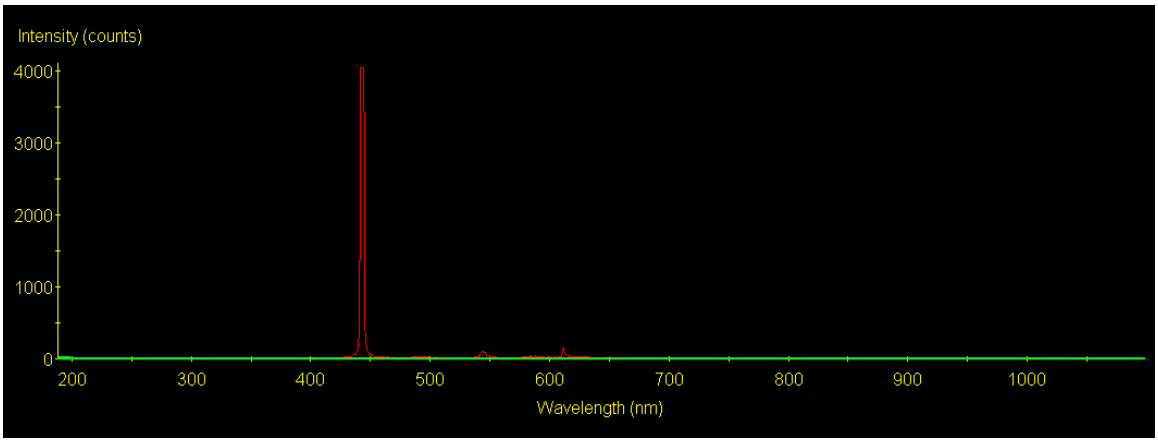

Figure 45. Measured output spectrum of the laser used in the engraver system.

According to above measured spectrum the laser used in this study has □=445nm output peak.

APPENDIX B. THRESHOLD OF CARBONIZATION

In order to determine the threshold of laser carbonization on polyimide and cardboard, laser system was tuned to different power level and then burned single dot on substrates. Figure 45 and Figure 46 demonstrate carbonization result on polyimide and card, respectively.

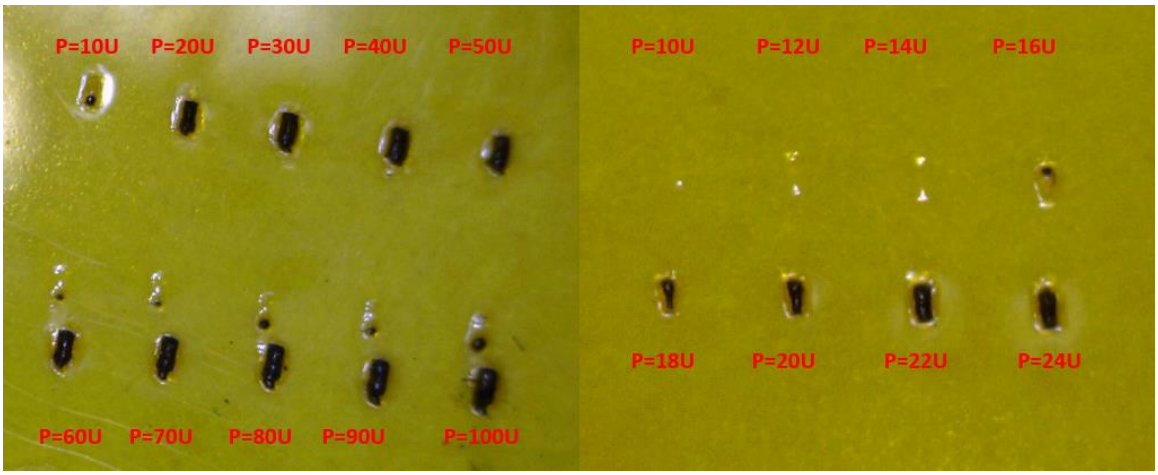

Figure 46. Single dot carbonization using various laser power on polyimide

According to test result indicated in Figure 45, laser beam started to carbonize polyimide when laser had power of 20 units, and the beam created a 0.05mm × 0.15mm carbonized area; moreover, measurement of carbonized area increased to 0.1mm × 0.2mm when laser was operated at power of 100 unit. Beam diameter and substrate thickness remains constant through the experiment, so carbonization area of single dot irradiation is also supposed to remain same. The increasing carbonization area is caused by energy spreading while energy increase. In this system, power of laser cannot be modified by tuning applied power; average output power is changed by varying duty

cycle. Therefore, threshold of polyimide carbonization in unit of *mJ/mm*^{2} can be calculated as below:

$$A_{carbonization} = 0.05 \times 0.15 = 0.0075mm^2$$

$$P_{electric}(P = 20\ unit\ power) = 0.35W$$

$$P_{optical} = P_{electric} \times efficacy = 0.35W \times 0.1 = 0.035W = 0.035\ J/s$$

$$E_{threshold} = \frac{P_{optical} \times t}{A_{carbonization}} = \frac{0.035J/s \times 0.00014s}{0.0075mm^2} = \mathbf{0.653mJ/mm^2}$$

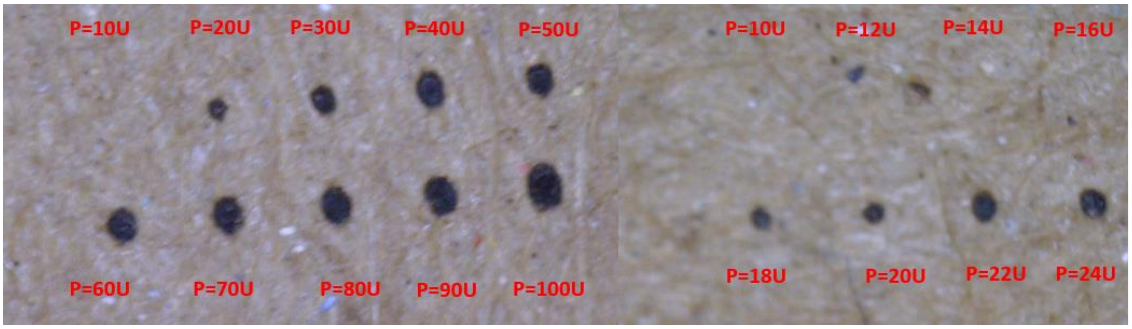

Figure 47. Single dot carbonization using various laser power on cardboard

Result of carbonization test on cardboard is presented in Figure 46. Carbonization started to occur stably when laser power is greater than 18%. Unit energy of carbonization threshold is calculated as below:

$$A_{carbonization} = 0.05 \times 0.07 = 0.0035mm^2$$

$$P_{electric}(P = 18\ unit\ power) = 0.33W$$

$$P_{optical} = P_{electric} \times efficacy = 0.33W \times 0.1 = 0.033W = 0.033J/s$$

$$E_{threshold} = \frac{P_{optical} \times t}{A_{carbonization}} = \frac{0.033J/s \times 0.00013s}{0.0035mm^2} = \mathbf{1.226\ mJ/mm^2}$$

APPENDIX C. POWER CONVERSION

This appendix can be used to convert between software given power units (U), which is a 8-bit binary input, and actual pulse width at the PWM output driving the laser.

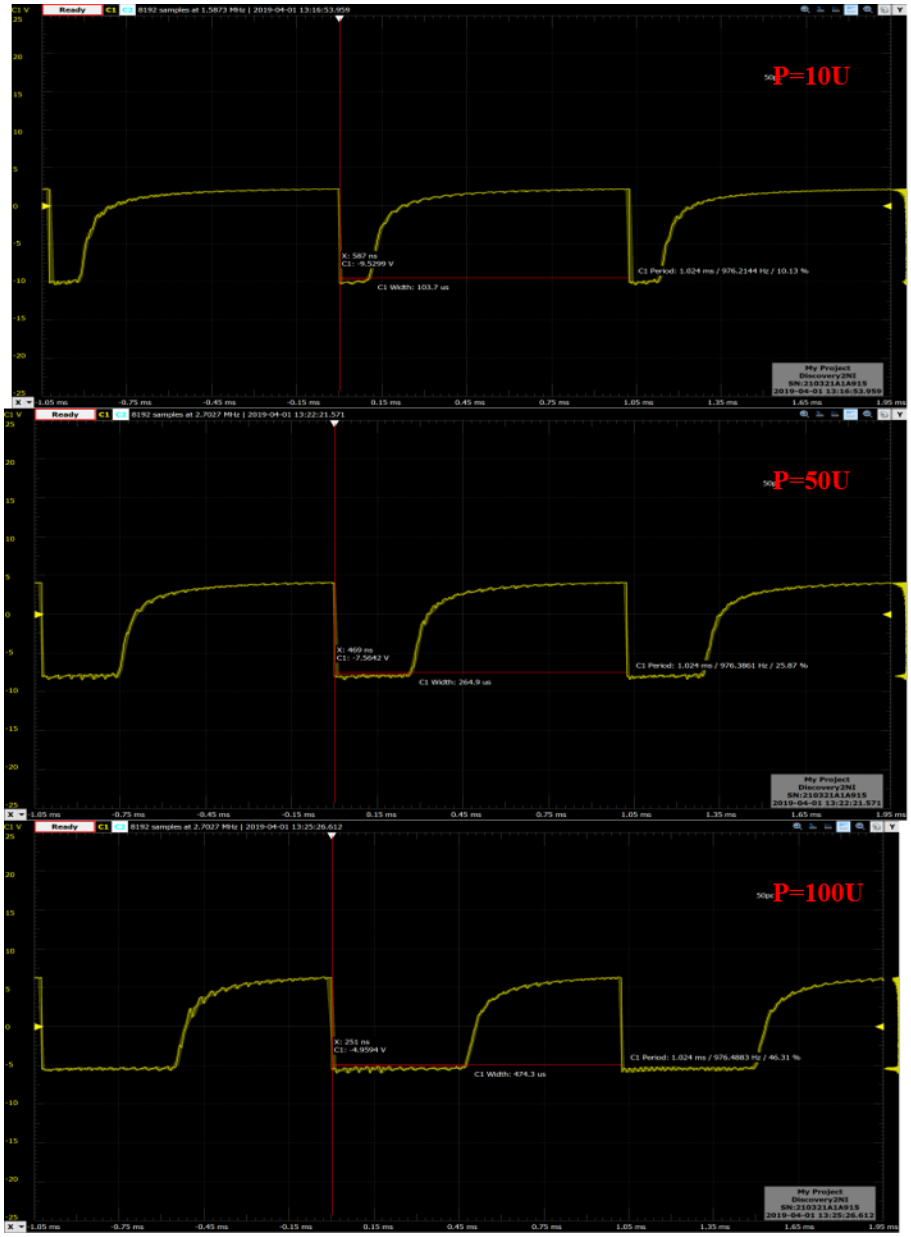

Figure 48. Waveform of PWM source driving laser when laser power was tuned to 10U, 50U, and 100U, respectively.

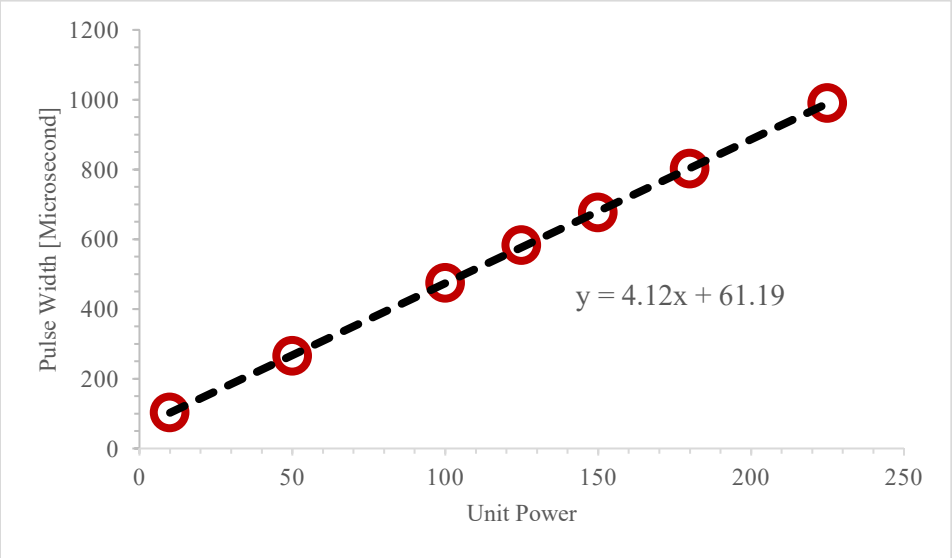

Figure 49. Correlation between power unit and pulse width

Base on the oscilloscope measurement presented in Figure 47, a linear correlation between unit power and pulse width could be found as Figure 48 shown. This can be established remembering that PWM signal period is 1024ms and the laser has full power of 2500mW in CW operation. Table 10 list the power conversion from unit power used in this work to actual electric power.

Table 10. Conversion from unit power to electric power

Unit Power (8-bit Register)	Pulse Width (μs)	Electric Power (W)
20	143.6	0.35
25	164.2	0.40
30	184.8	0.45
35	205.4	0.50
40	226.1	0.55
45	246.6	0.60
50	267.2	0.65
55	287.8	0.70
60	308.4	0.75
65	329.9	0.80
70	349.6	0.85
75	370.2	0.90
80	390.8	0.95
85	411.4	1.00
90	432.0	1.05
95	452.6	1.10
100	473.2	1.15

APPENDIX D. ADDITIONAL CARBONIZATION RESULT OF VARIOUS CELLULOSE-BASED MATERIAL

This appendix shows the type of paper products attempted but not found successful for LSC formation. The final paper used in this study is named *50 lb. chipboard* (Grafix®), available via Amazon.com. All paper results are obtained using this chipboard paper.

Table 11. Carbonization result of various cellulose-based material

Name or Trade Marker of Substrate	**Carbonization Result**
Biose® X-9® Multi-Use Copy Paper	Laser lighted up the substrate
Whatman ® No.1 Chromatography Paper	Laser Lighted up the substrate
HP® Everyday Glossy Photopaper	Negative
Canon® PP-301Photopaper	Negative, glossy surface had minor damage
Powercoat® HD	Negative, minor color change can be seen
Powercoat® XD	Negative

Thesis and Dissertation Services